Topological Protectorates of Fermi Surfaces

Christian Pfleiderer

Physik-Department
Technische Universität München

Collaborations

Munich

M. Wilde

N. Huber
G. Causer
L. Worch
M. Dodenhöft
A. Niedermayr

A. Bauer

G. Benka

Stuttgart

A. Schnyder

M. Hirschmann
K. Alpin

Zoology of Topological Materials

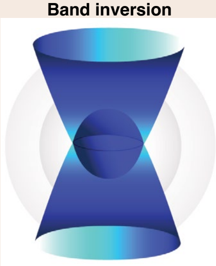

Topological insulators

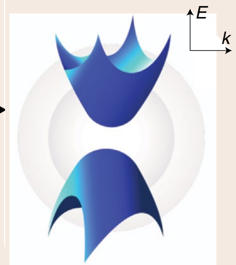

Classification	Symmetry	Band inversion
Z_2	Time reversal	Odd times
High order	Crystalline symmetry	Even times
Crystalline TI	Crystalline symmetry	≥1

Dirac and Weyl semimetals

Classification	Symmetry	Band crossing
Dirac semimetal	Rotation	Rotation axis
Weyl semimetal (non-magnetic)	Inversion symmetry broken	Accidental degenerate point
Weyl semimetal (ferromagnetic)	Time reversal broken	

New fermions

Nodal line semimetal	Mirror	Mirror plans
	Non-symmorphic	Brillouin zone edge
New fermion	Rotation and non-symmorphic	High-symmetry point
Chiral topology	Mirror symmetry broken	Arbitrary point (chiral Weyl fermion)
		High-symmetry point (multiple Fermion)

M. G. Vergniory et al., Nature **586** 480 (2020)
Y. Xu et al., Nature 586 **702** (2020)
P. Narang et al., Nat. Mat. AOP (2020)

Zoology of Topological Materials

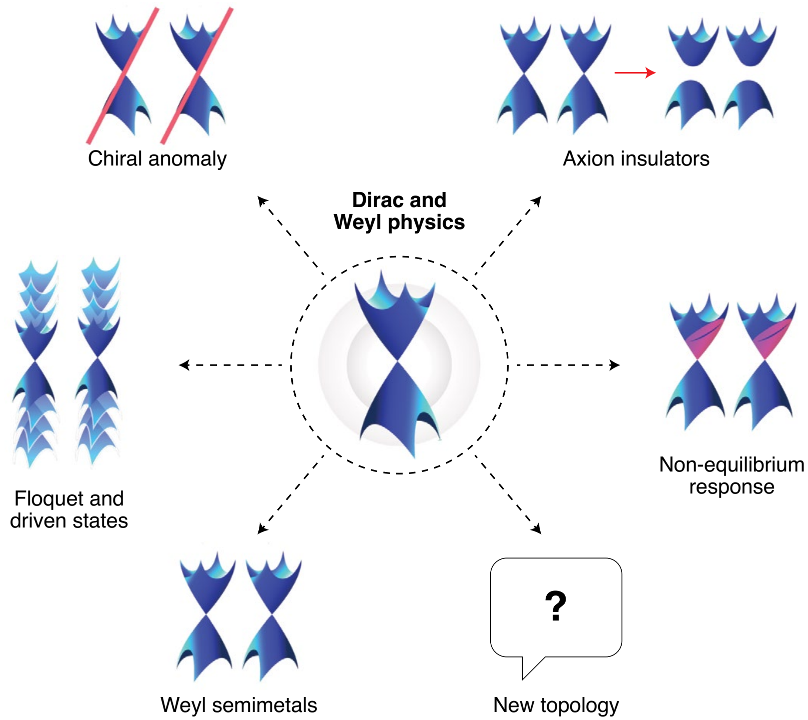

the ideal Weyl metal wish list

- single pair of Weyl points
- located at EF (or very close)
- far separated in k-space
- no topologically trivial bands

M. G. Vergniory et al., Nature **586** 480 (2020)
Y. Xu et al., Nature 586 **702** (2020)
P. Narang et al., Nat. Mat. AOP (2020)

Outline

- Topological Fermions in TM-Silicides
- Topological protectorates in CoSi
- Topological protectorates in MnSi

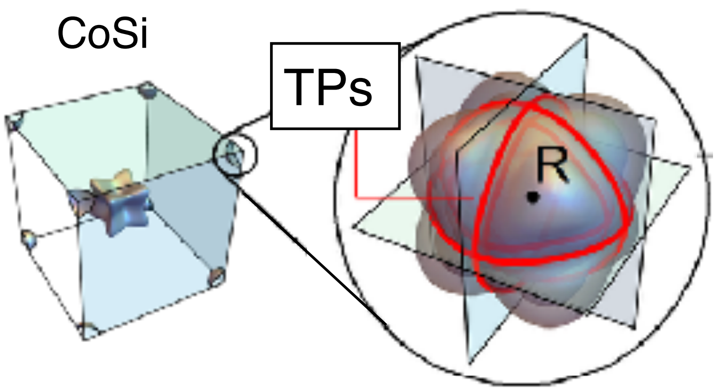

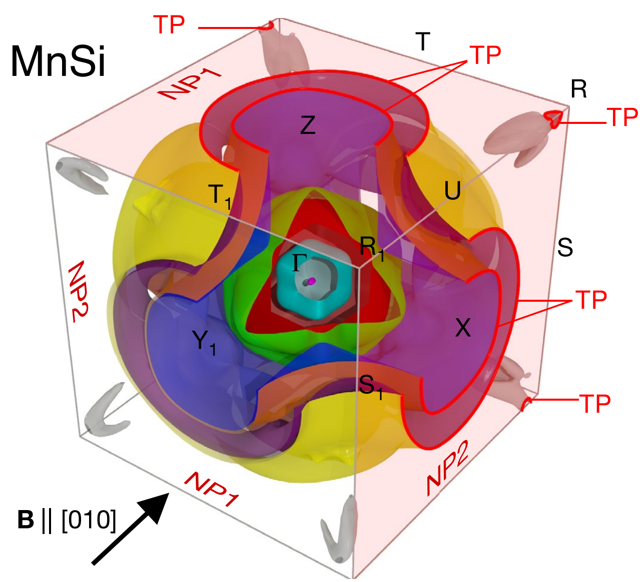

Huber et al., arXiv/2107.02820

Wilde et al., Nature **594**, 374 (2021)

Topological Fermions
in Transition Metal Silicides

Multi-fold degeneracies in chiral crystals

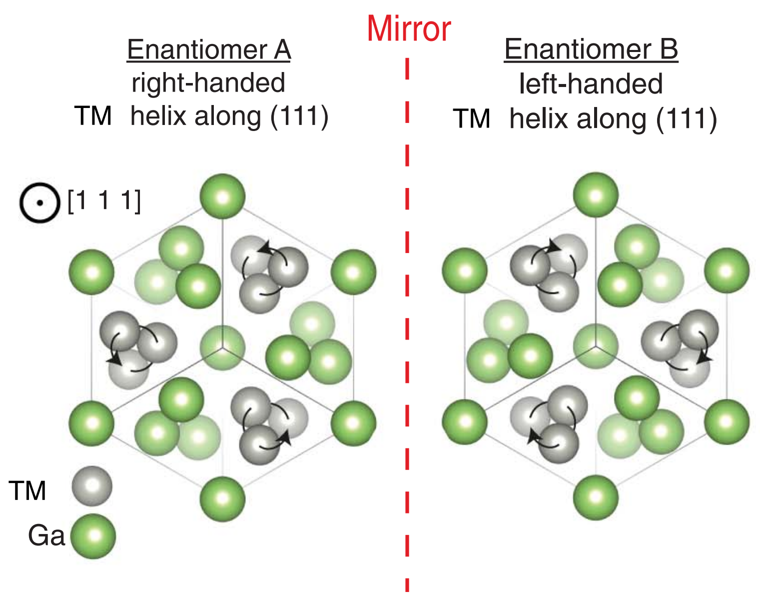

$$H = \delta \boldsymbol{k} \cdot \boldsymbol{S}$$

$$\delta \boldsymbol{k} = \boldsymbol{k} - \boldsymbol{k}_0$$

$$[\boldsymbol{S}_i, \boldsymbol{S}_j] = i\epsilon_{ijk}\boldsymbol{S}_k$$

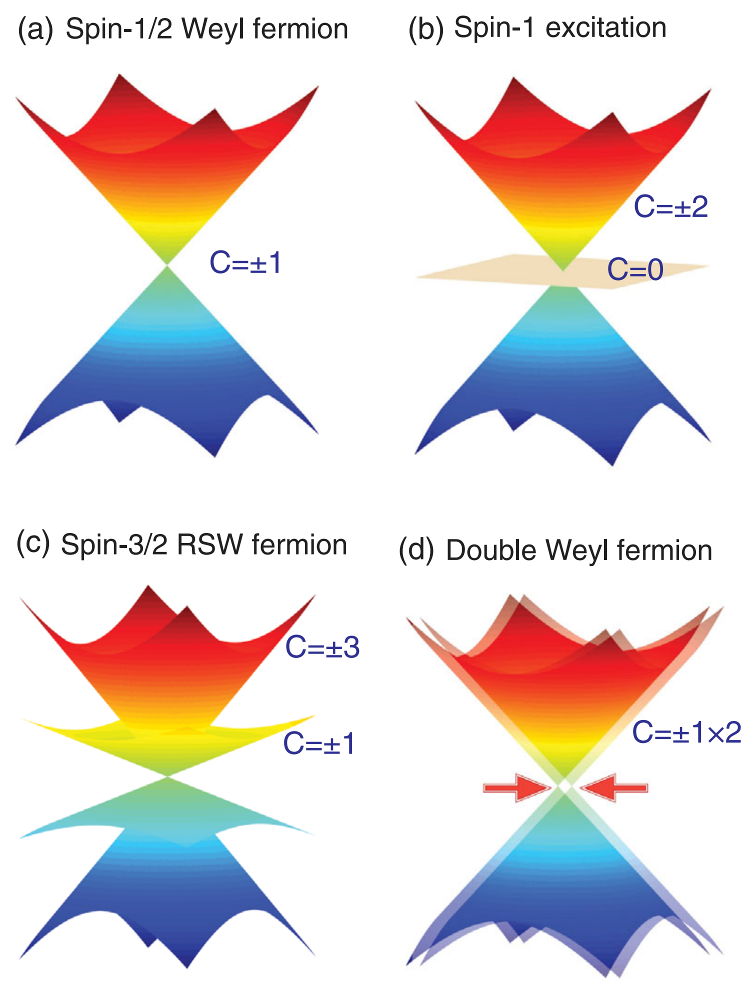

Peizhe Tang et al., PRL **119** 206402 (2017)

Topological Fermions in Transition Metal Silicides

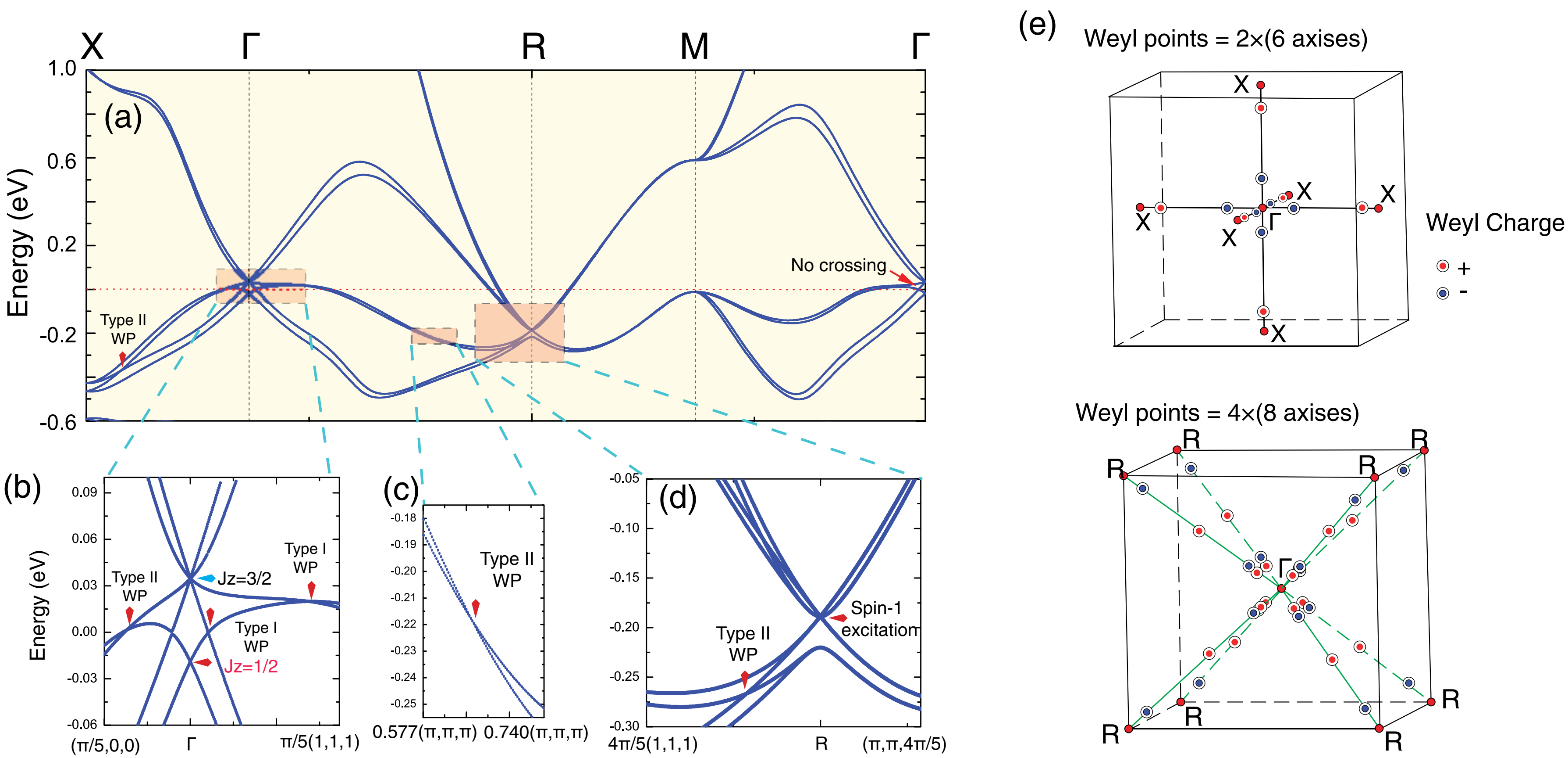

Peizhe Tang et al., PRL **119** 206402 (2017)

Topological Fermions in Transition Metal Silicides

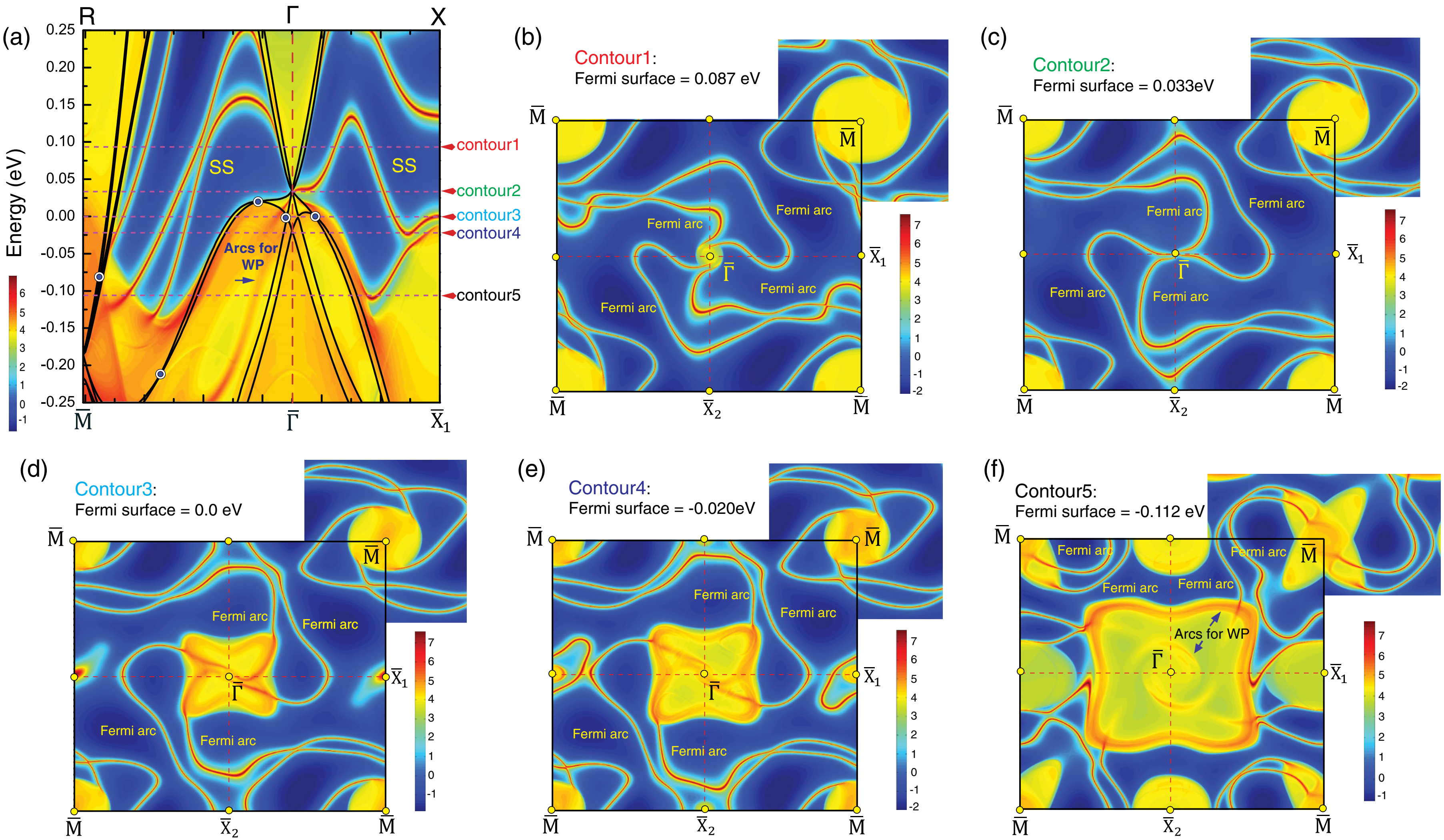

Peizhe Tang et al., PRL **119** 206402 (2017)

ARPES of chiral fermions and long Fermi arcs in CoSi

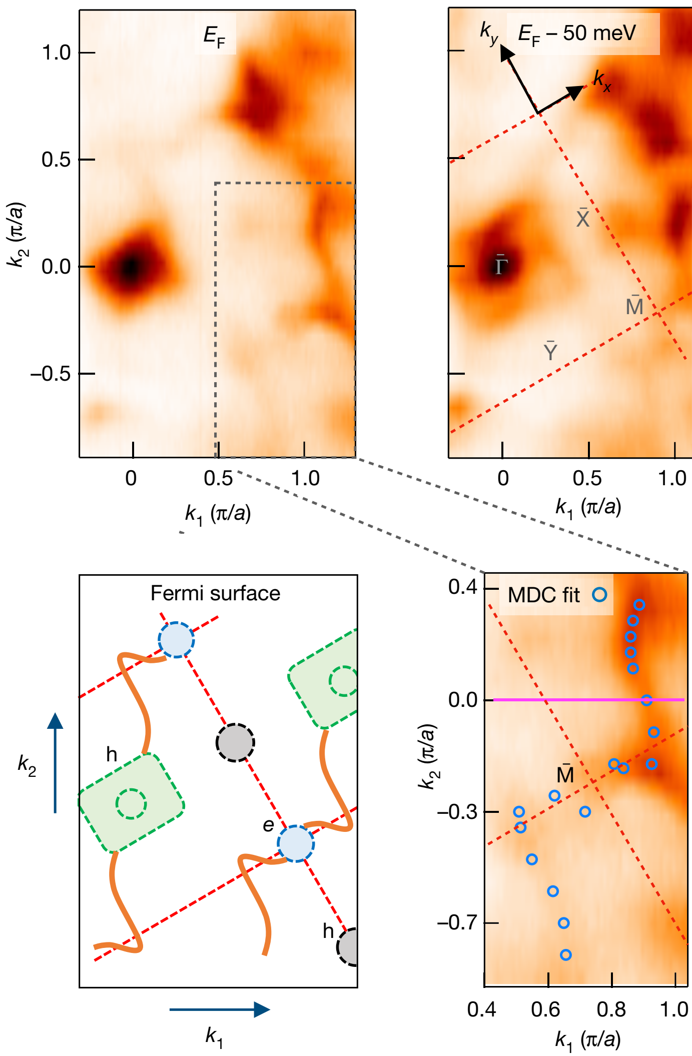

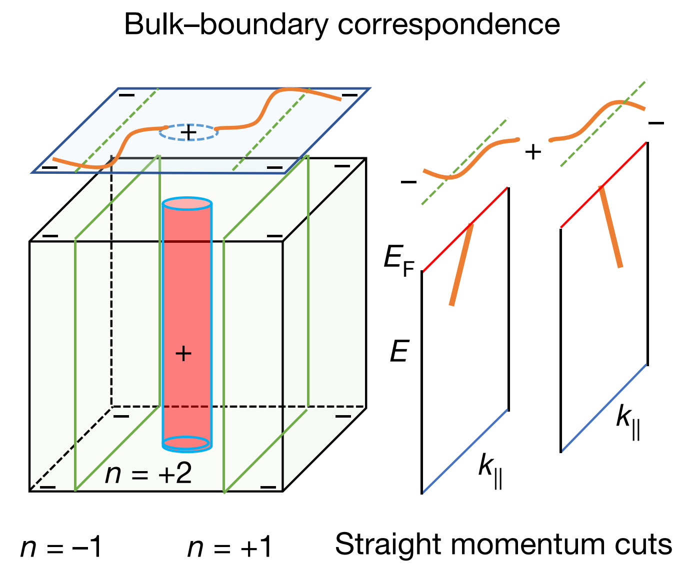

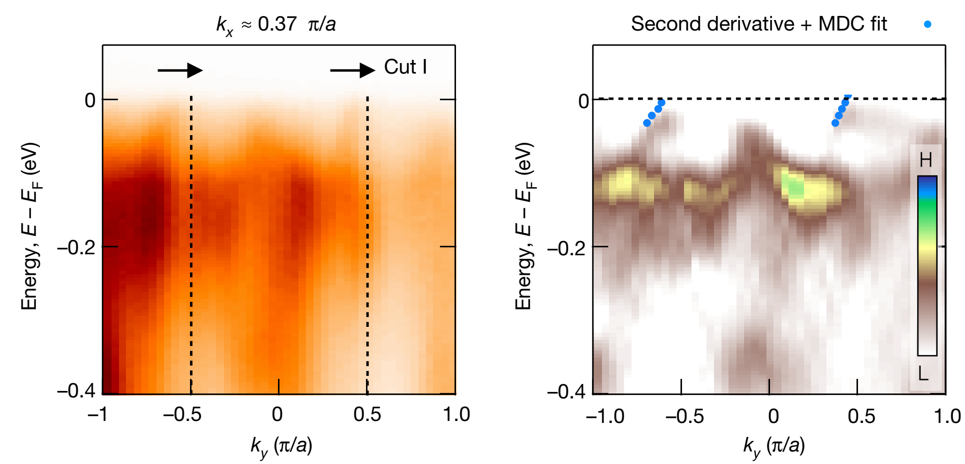

Sanchez et al., Nature **597** 500 (2019)
Zhicheng Rao et al., Nature **597** 496 (2019)

ARPES of chiral fermions and long Fermi arcs in CoSi

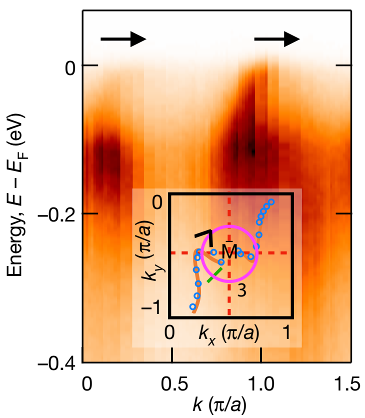

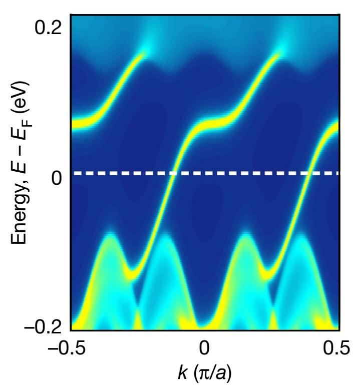

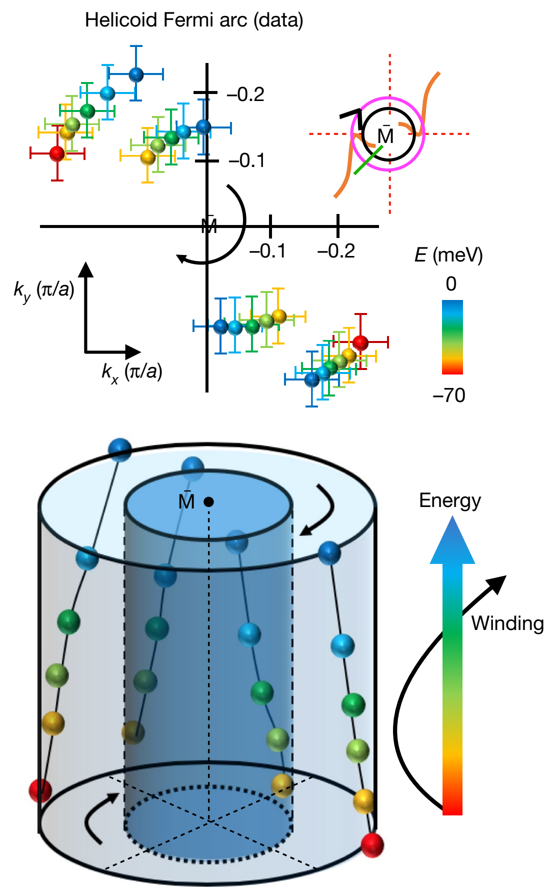

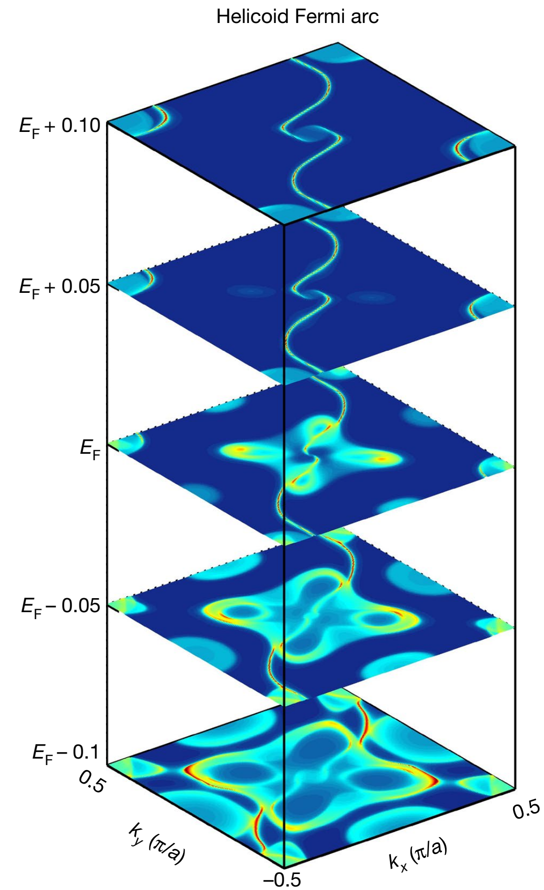

Sanchez et al., Nature **597** 500 (2019)
Zhicheng Rao et al., Nature **597** 496 (2019)

Quantum Oscillations in CoSi

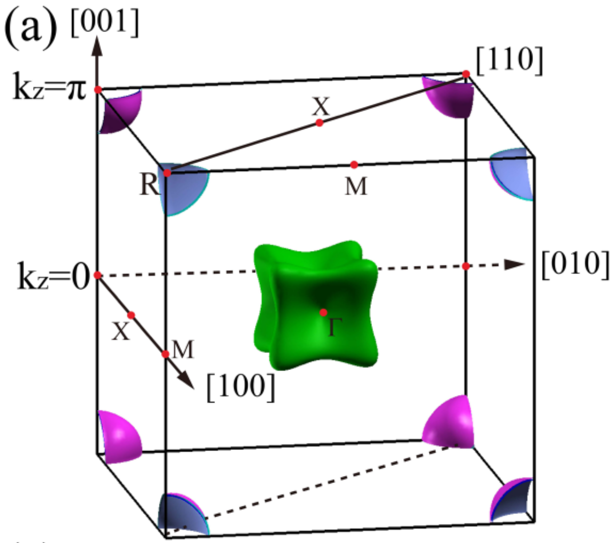

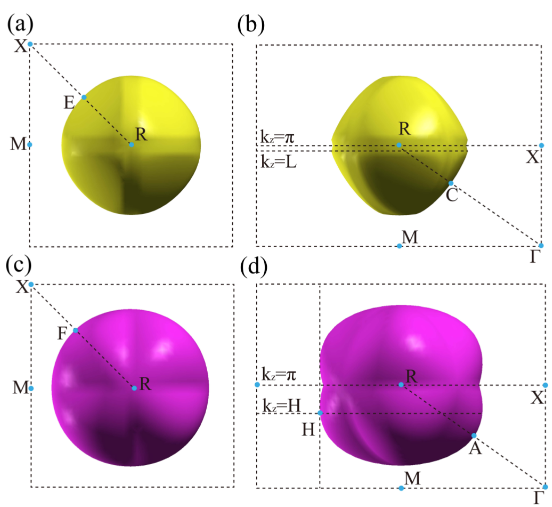

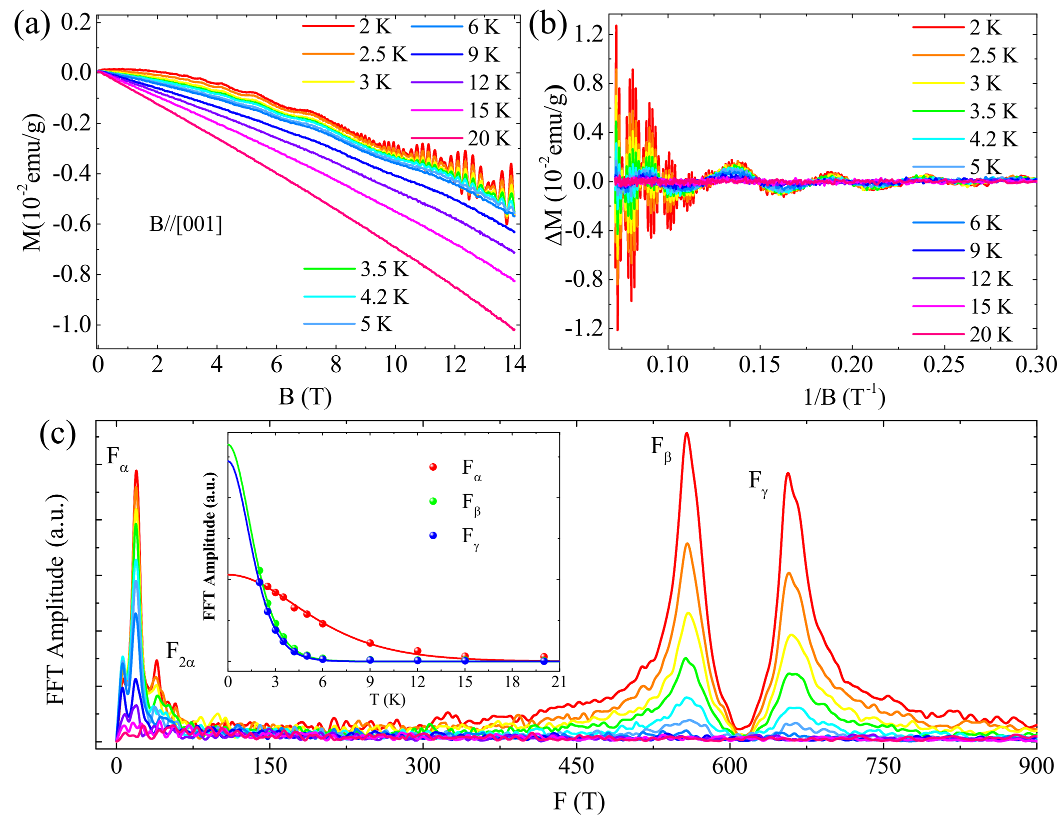

Huan Wang et al., PRB **102** 115129 (2020)
D.S. Wu et al., Chin. Phys. Lett. **36** 077102 (2019)
Xitong Xu et al., PRB **100** 045104 (2019)

Maximal Chern numbers in PdGa

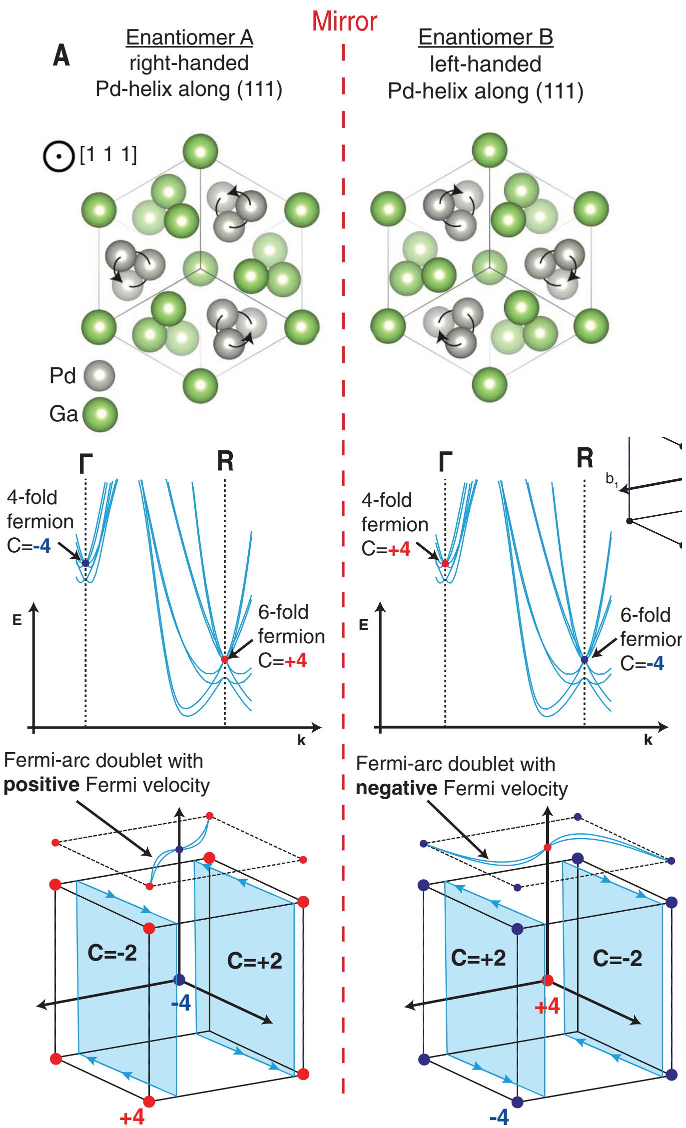

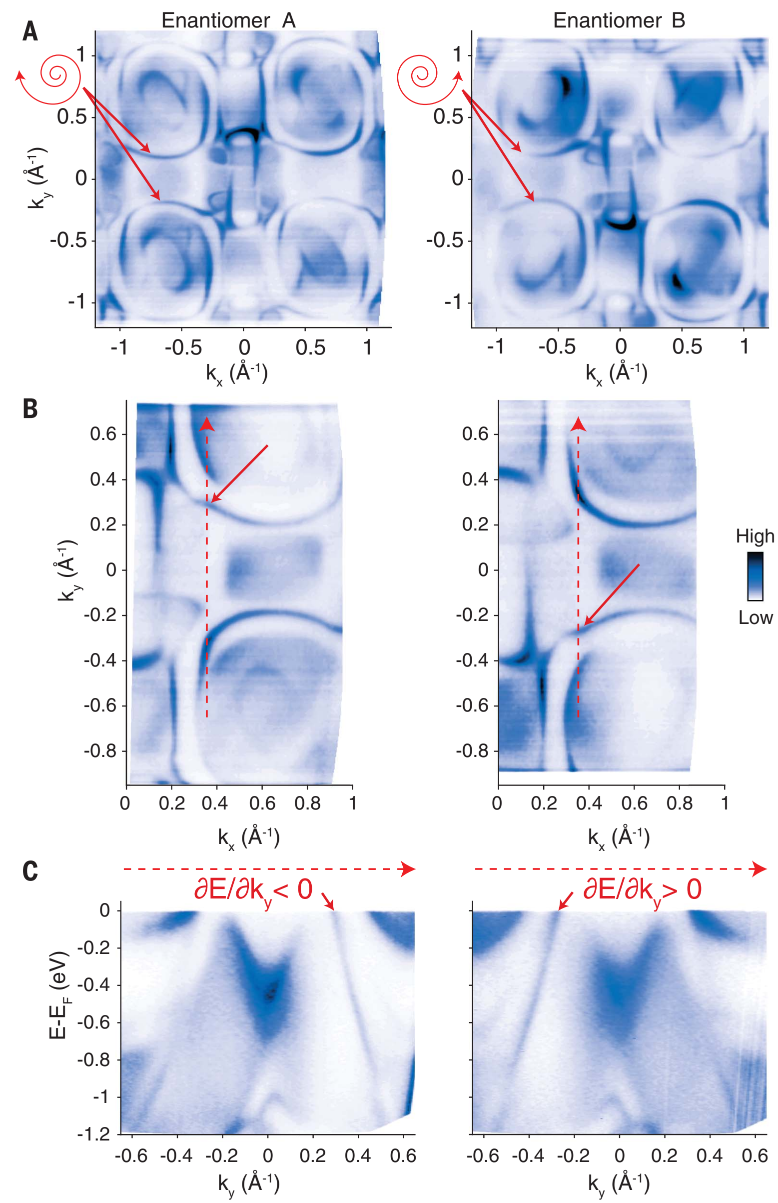

Schröter et al., Science **369** 179 (2020)

Band sticking in SG198

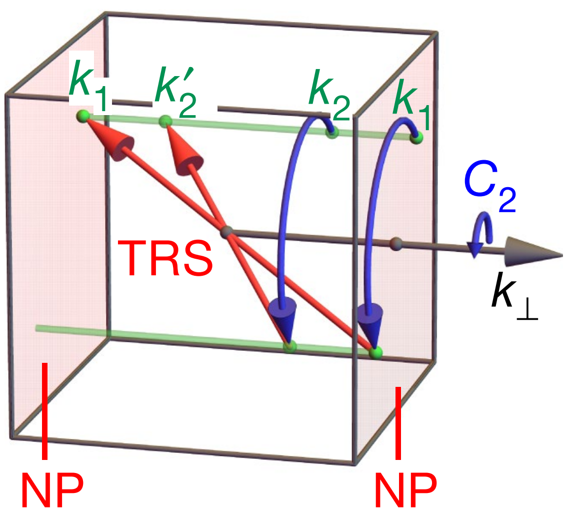

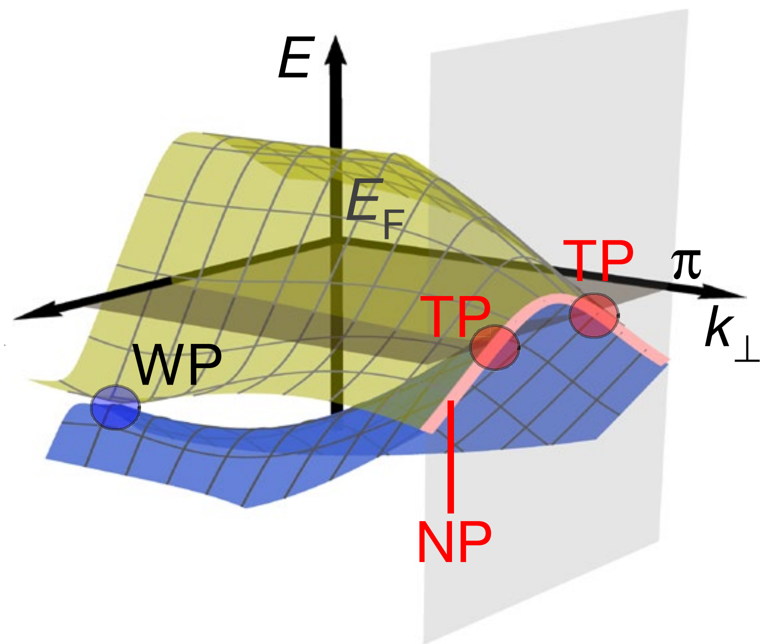

11. Nielsen, H. B. & Ninomiya, M. Absence of neutrinos on a lattice (I). Proof by homotopy theory. *Nucl. Phys. B* **185**, 20–40 (1981).
12. Nielsen, H. B. & Ninomiya, M. Absence of neutrinos on a lattice (II). Intuitive topological proof. *Nucl. Phys. B* **193**, 173–194 (1981).

Nielsen, Ninomiya, Nucl. Phys. B **185** 20 (1981)
Nielsen, Ninomiya, Nucl. Phys. B **193** 173 (1981)
Z.-M. Yu et al., PRB **100** 041118 (2019)

Wilde, et al., Nature **594**, 374 (2021)

Single-Weyl point & Nodal planes in PtGa

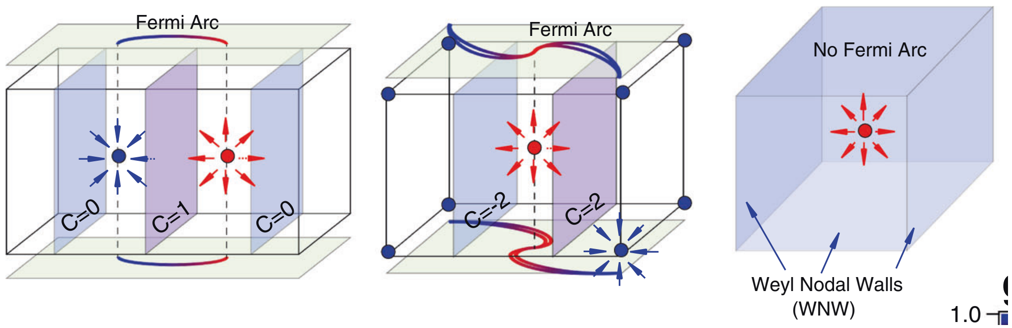

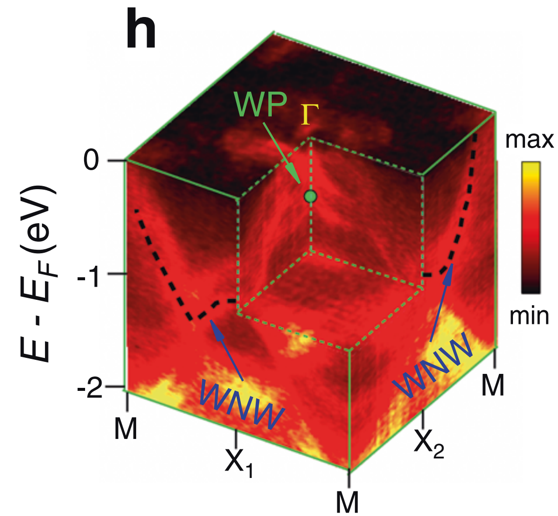

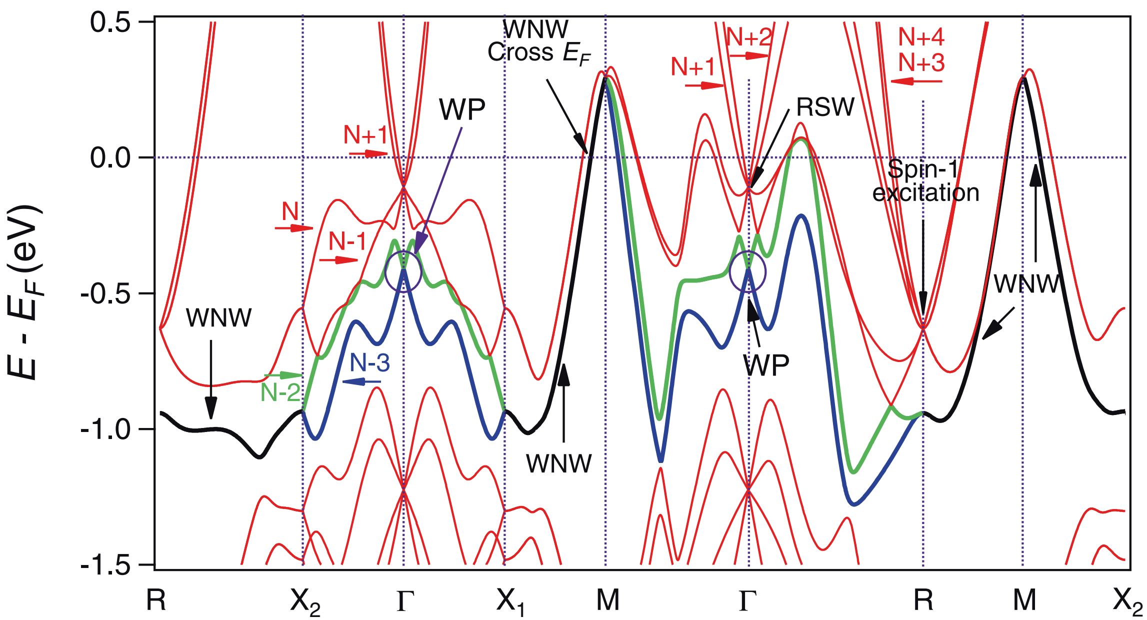

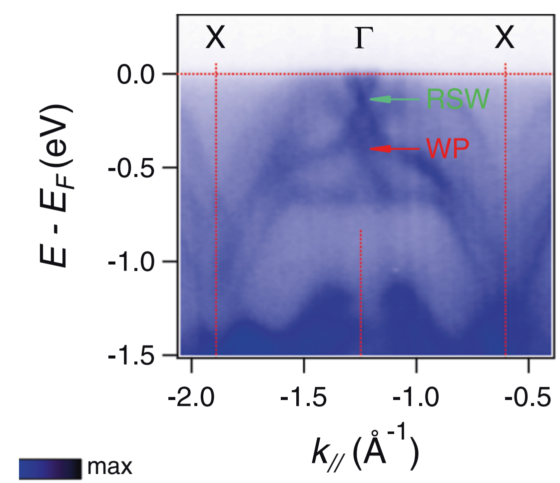

J.-Z. Ma et al., Nat. Comms. **12** 3994 (2021)

Z.-M. Yu et al., PRB **100** 041118 (2019)

Band sticking in non-symmorphic crystals

hexagonal closed-packed

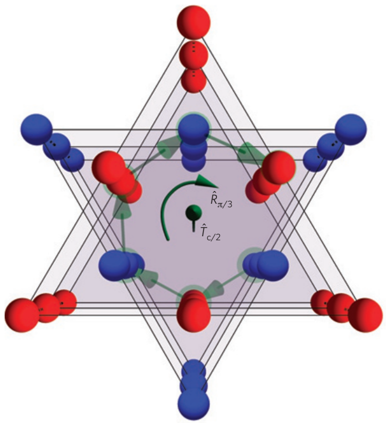

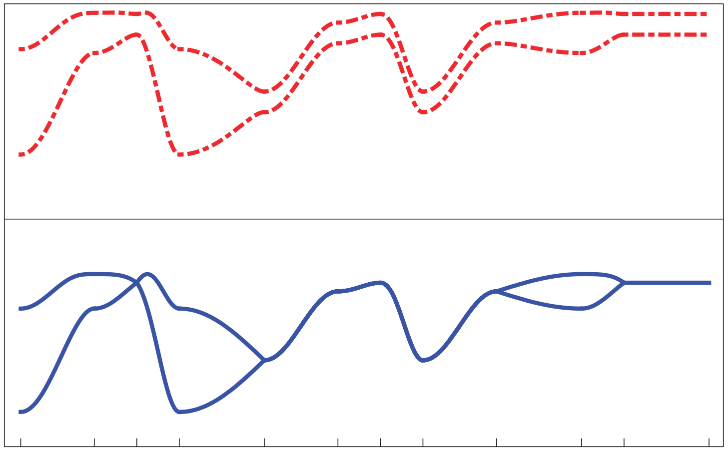

Table 1 | Some non-symmorphic groups and their ranks, colloquial structure names and representative materials.

d	Name	Examples	Space group	$\mathcal{S}$
2	Shastry–Sutherland	$SrCu_2(BO_3)_2$	*p4g*	2
3	hcp	Be, Mg, Zn	$P6_3/mmc$	2
3	Diamond	C, Si	$Fd\bar{3}m$	2
3	Pyrochlore	$Dy_2Ti_2O_7$ (spin ice)	$Fd\bar{3}m$	2
3	–	α-SiO_2, GeO_2	$P3_121$	3
3	–	$CrSi_2$	$P6_222$	3
3	–	$Pr_2Si_2O_7$, $La_2Si_2O_7$	$P4_1$	4
3	Hex. perovskite	$CsCuCl_3$	$P6_1$	6

Parameswaran et al., Nat. Phys. **9** 299 (2013)

Topological Nodal Surfaces in Acoustic Crystals

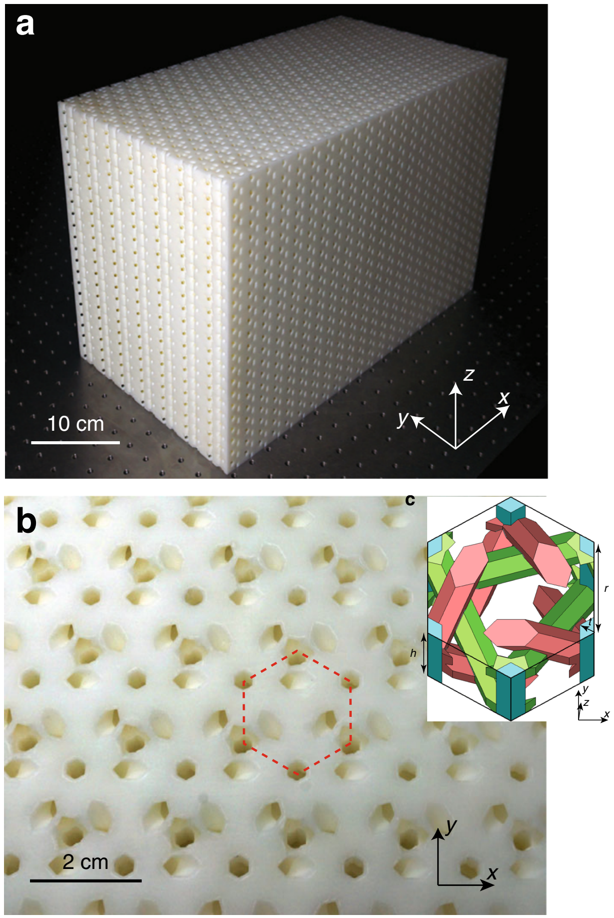

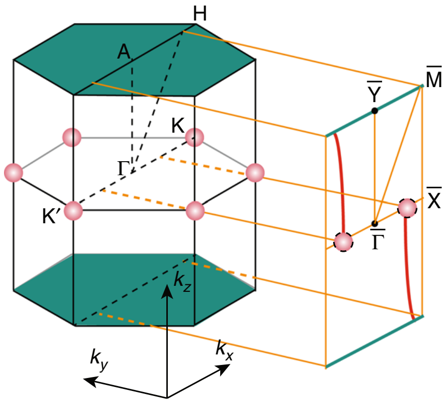

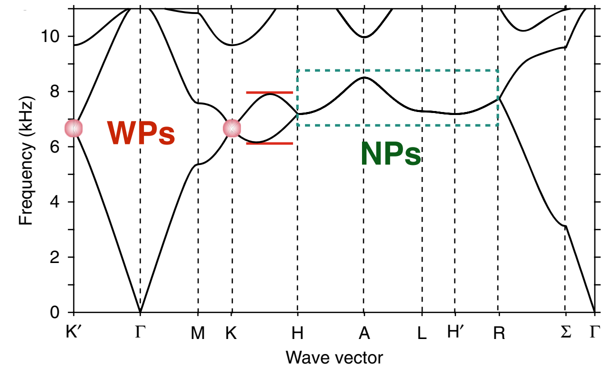

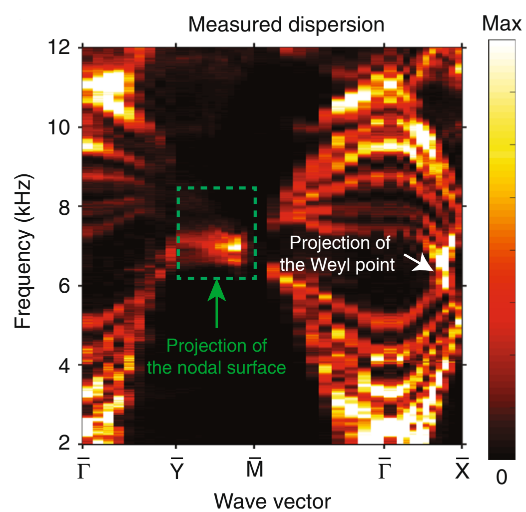

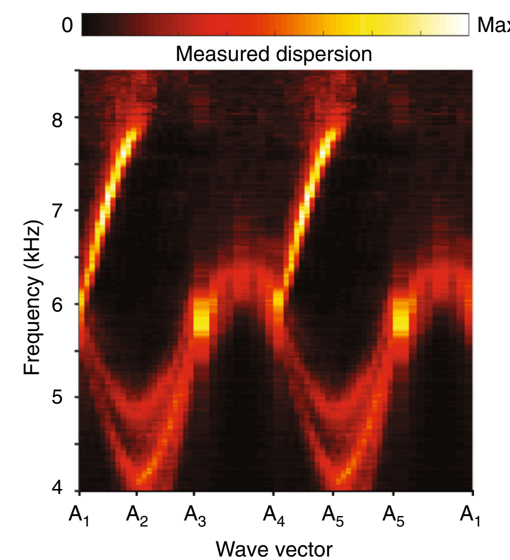

Yihao Yang et al., Nat. Comms. **10** 5185 (2019)

Meng Chiao et al., Sci. Adv. **6** eeav2360 (2020)

Quantum Oscillations in Metals

Electron beam in a magnetic field

Cathode Ray Tube

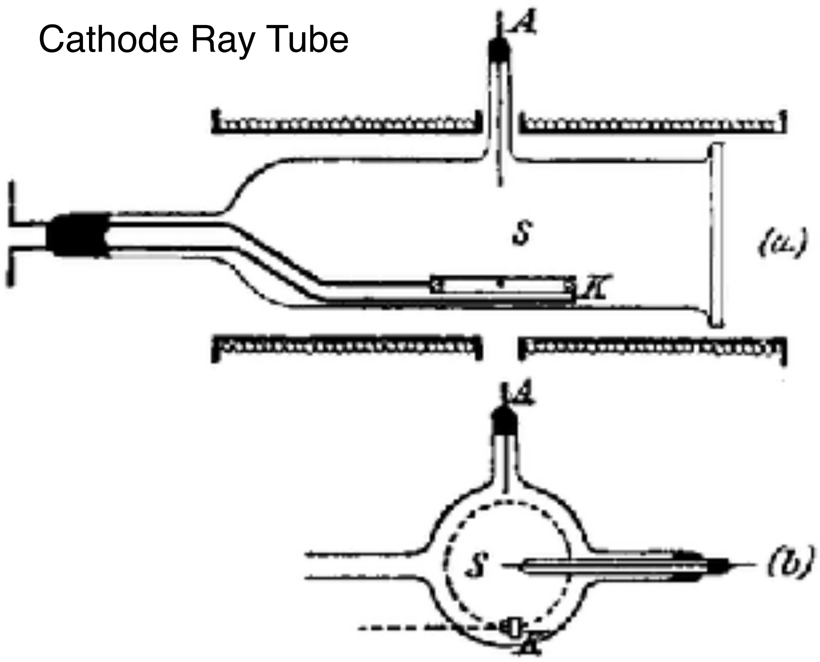

Wehnelt, Ann. Physik **14**, 462 (1904)

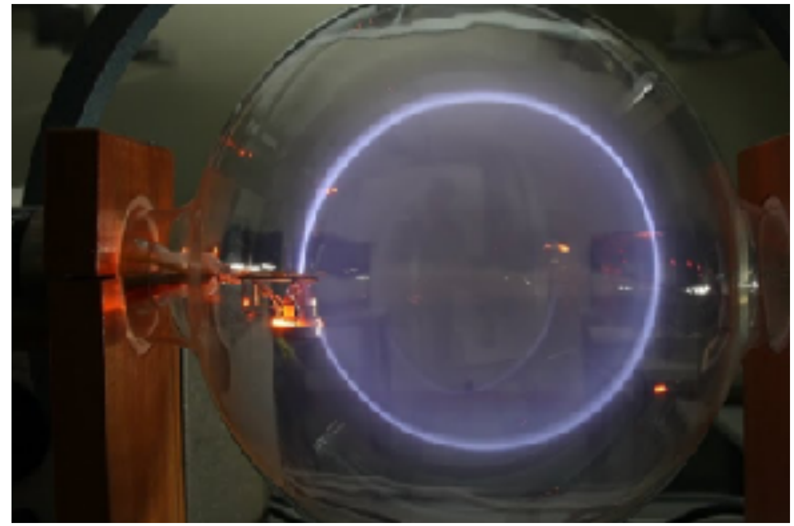

Physik LK 14 - e/m - Bestimmung / Fadenstrahlrohr (Benno Köhler)

http://www.uranmaschine.de/43200.Fadenstrahlrohr/Fadenstrahlrohr_Aufnahme_11_hires.jpg

Semi-classical electron motion & Landau quantisation

B=0

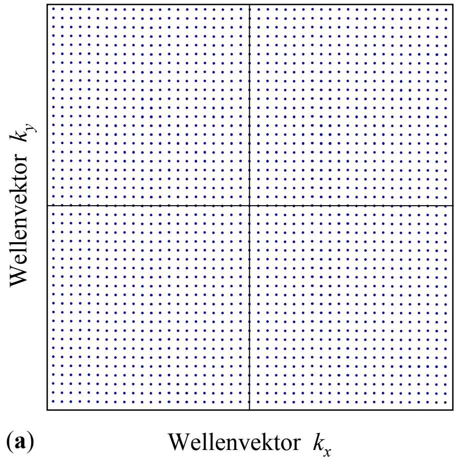

(a)

Landau quantisation

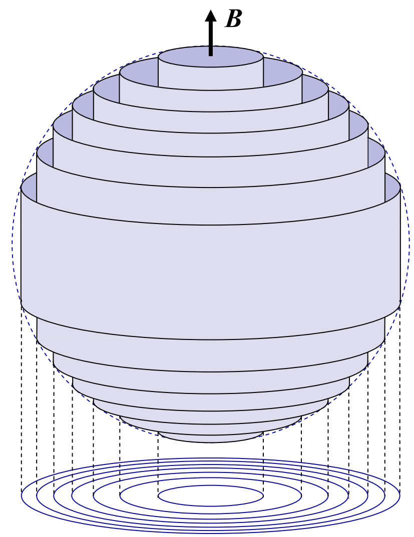

Fermi surface of Gold

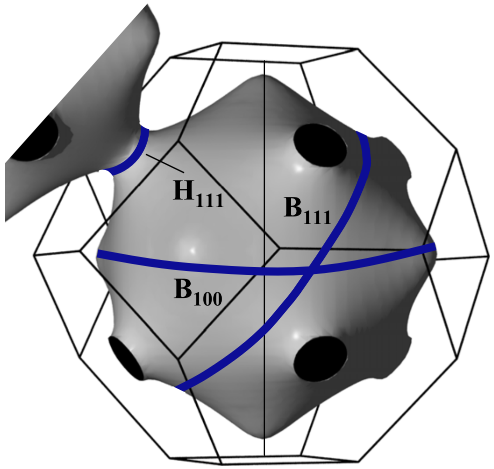

B>0

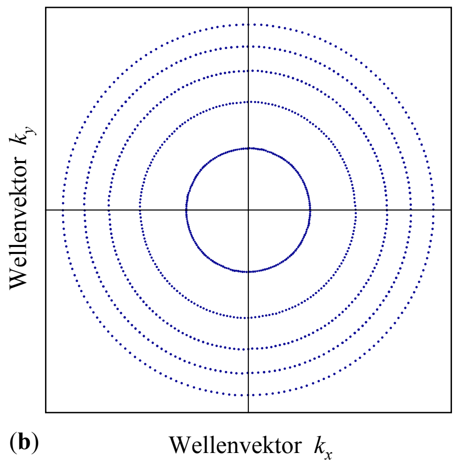

(b)

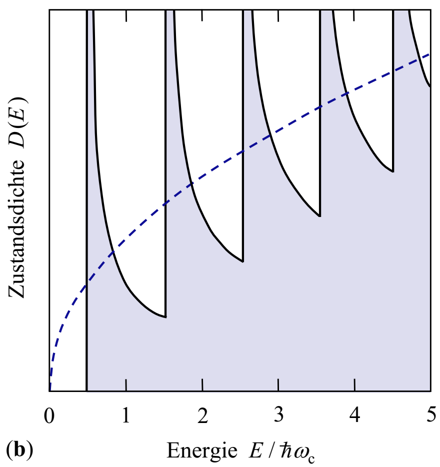

(b)

quantum oscillations

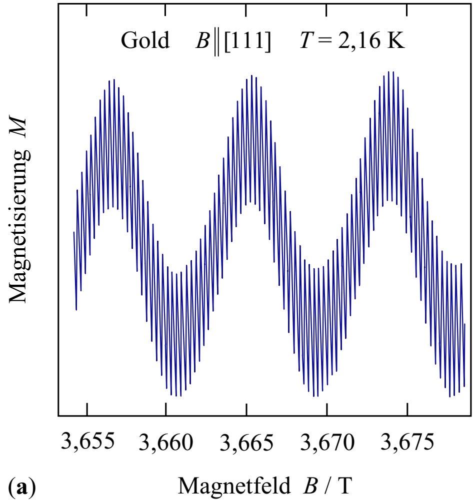

(a)

S. Hunklinger (textbook on solid state physics)

Key information contained in quantum oscillations

Reciprocal space trajectory

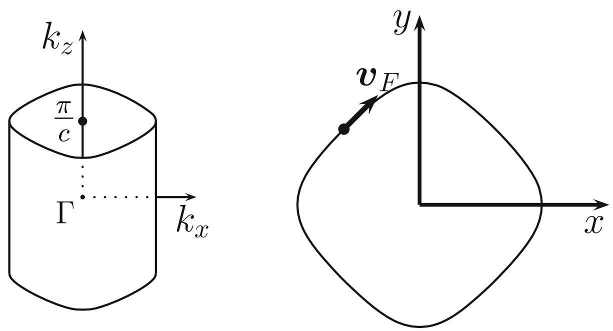

Real space trajectory

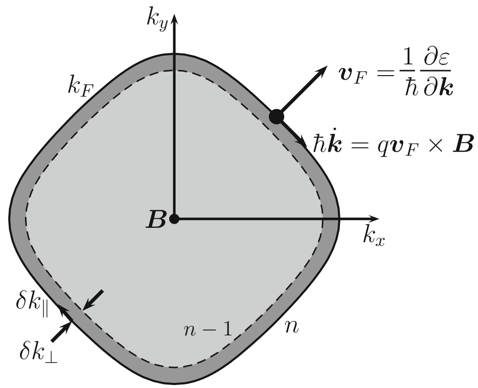

$$\Delta\left(\frac{1}{B}\right) \equiv \frac{1}{B_n} - \frac{1}{B_{n-1}} = \frac{2\pi e}{\hbar \mathcal{A}}$$

Onsager: $F = \dfrac{\hbar \mathcal{A}}{2\pi e}$

Effects of finite temperature

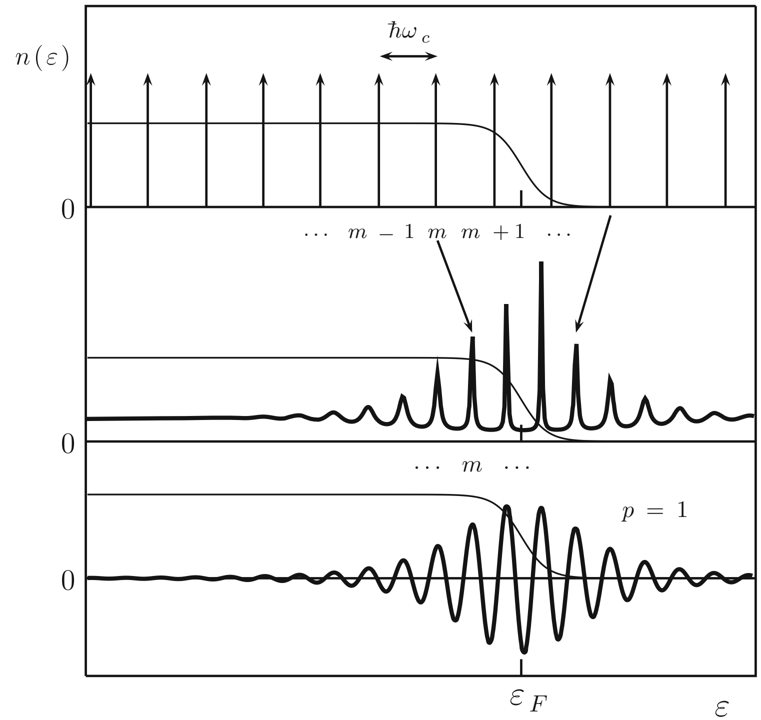

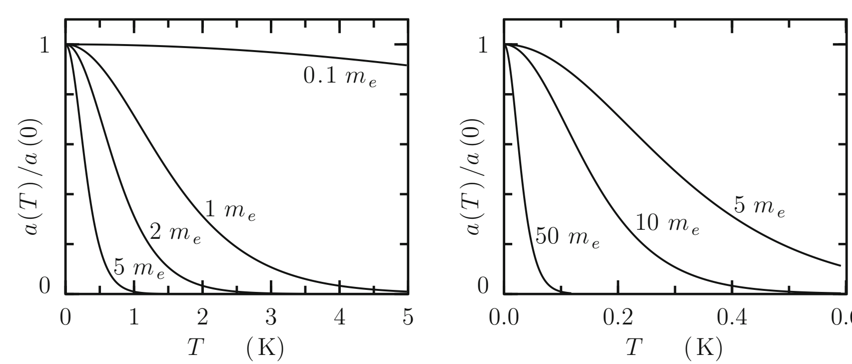

S. R. Julian, Solid-State Sciences **180**, 137 (2015)

Magnetic Breakdown

Free electron orbits

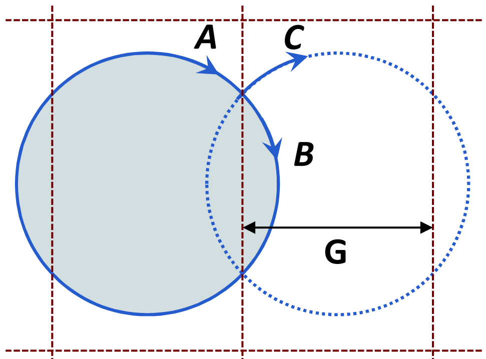

Chambers formula

$$P = e^{-H_0/H}$$

$$H_0 = \frac{\pi \hbar c}{e} \left(\frac{k_g^3}{a+b} \right)^{1/2}$$

breakdown field

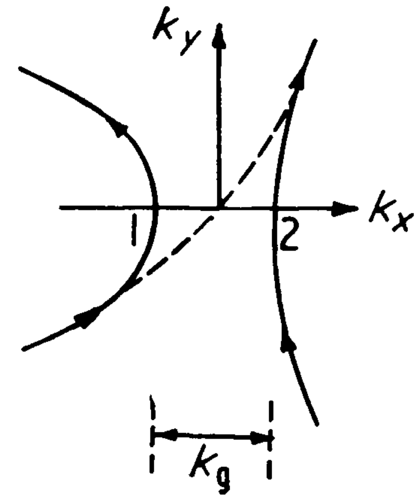

Shoenberg, Magnetic Oscillations in Metals

Electron orbits in a lattice

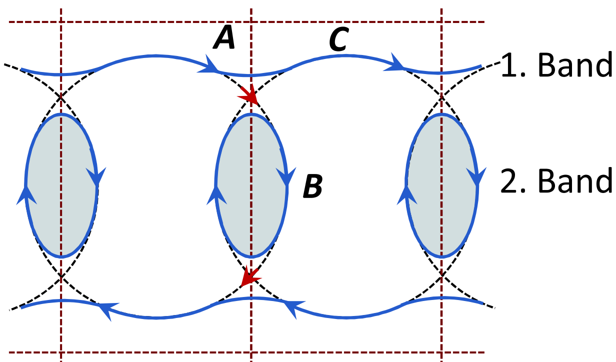

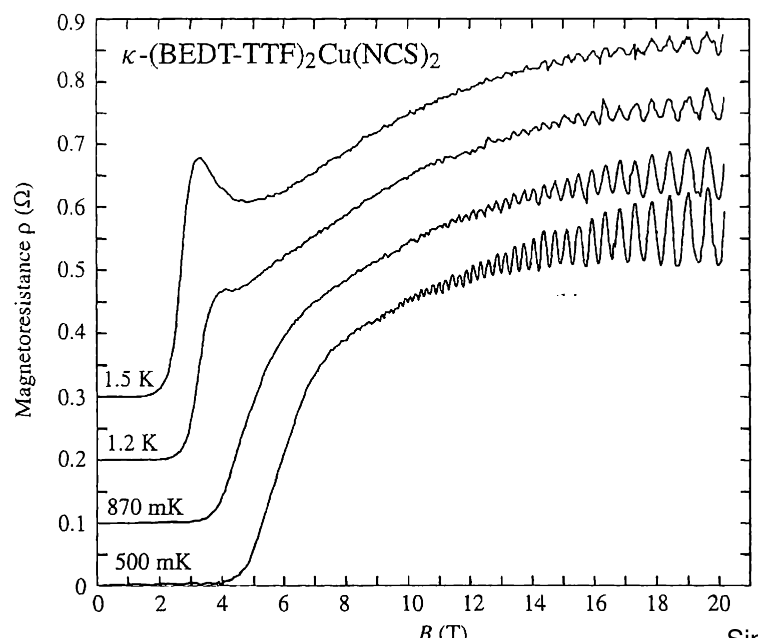

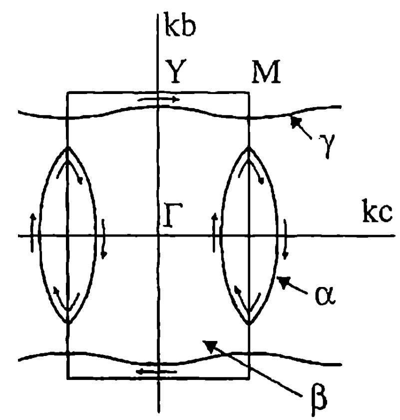

Gross-Marx, Solid-State-Physics

Singleton, Oxford Master Series

Topological Protectorates in CoSi

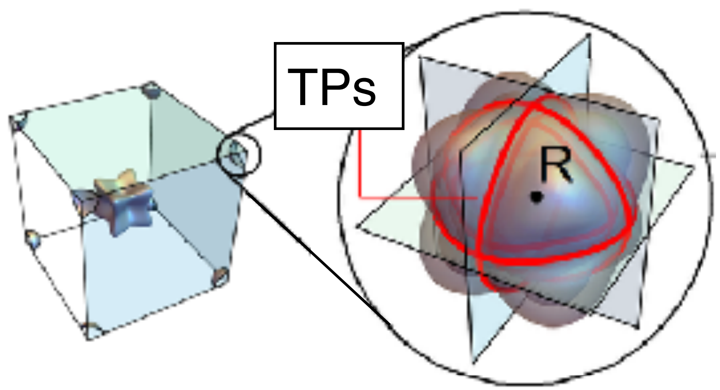

DFT band structure of CoSi with SOC

Band index	Γ	M	R	NP
1	+1	-	-	-1
2	-1	-2	-	+1
3	+3	-	-	-13
4	+1	+2	-4	+13
5	-1	-	-	-5
6	-3	+2	0	+5
7	-3	-	-	-1
8	-1	-2	+4	+1

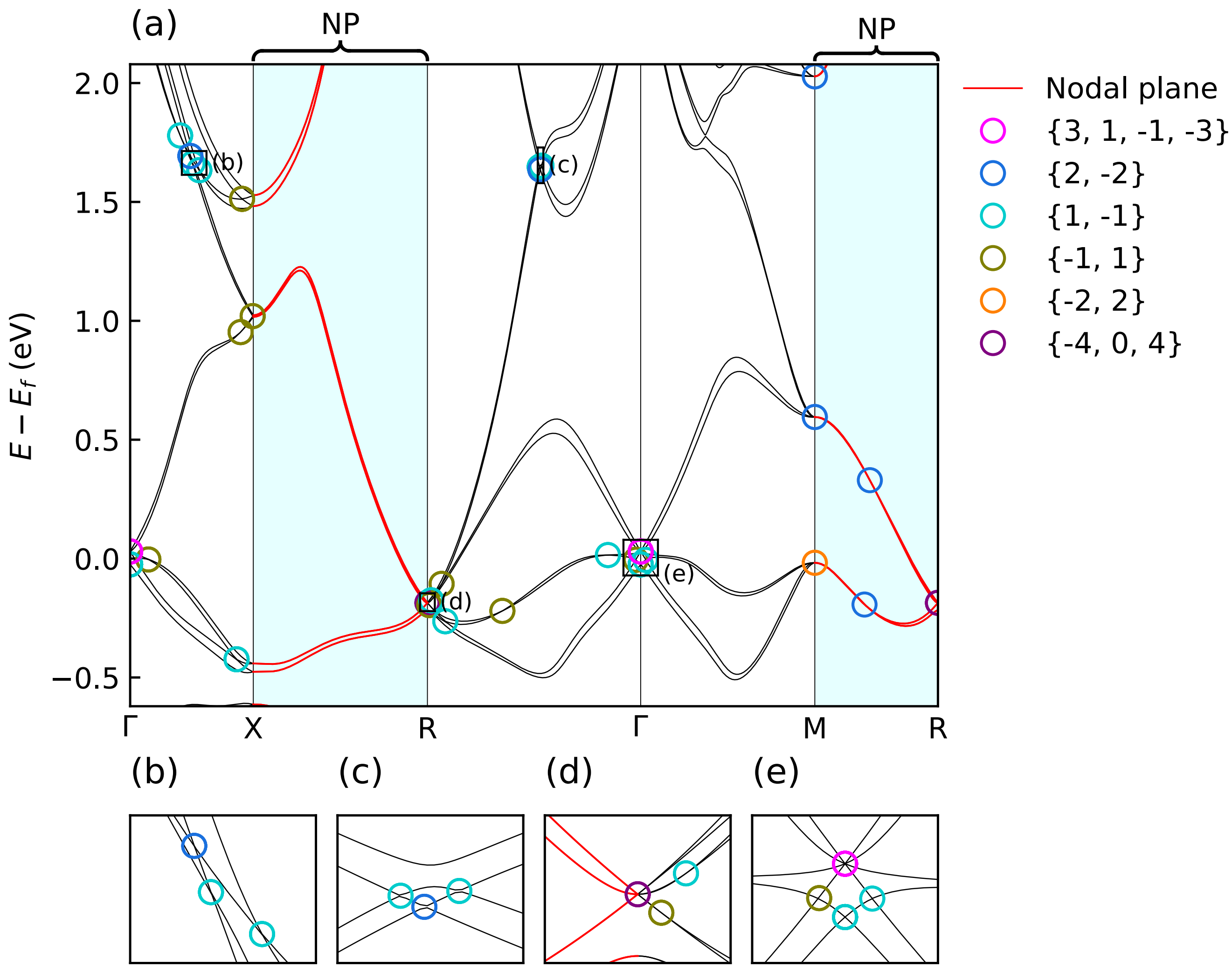

Generic tight-binding model of SG198

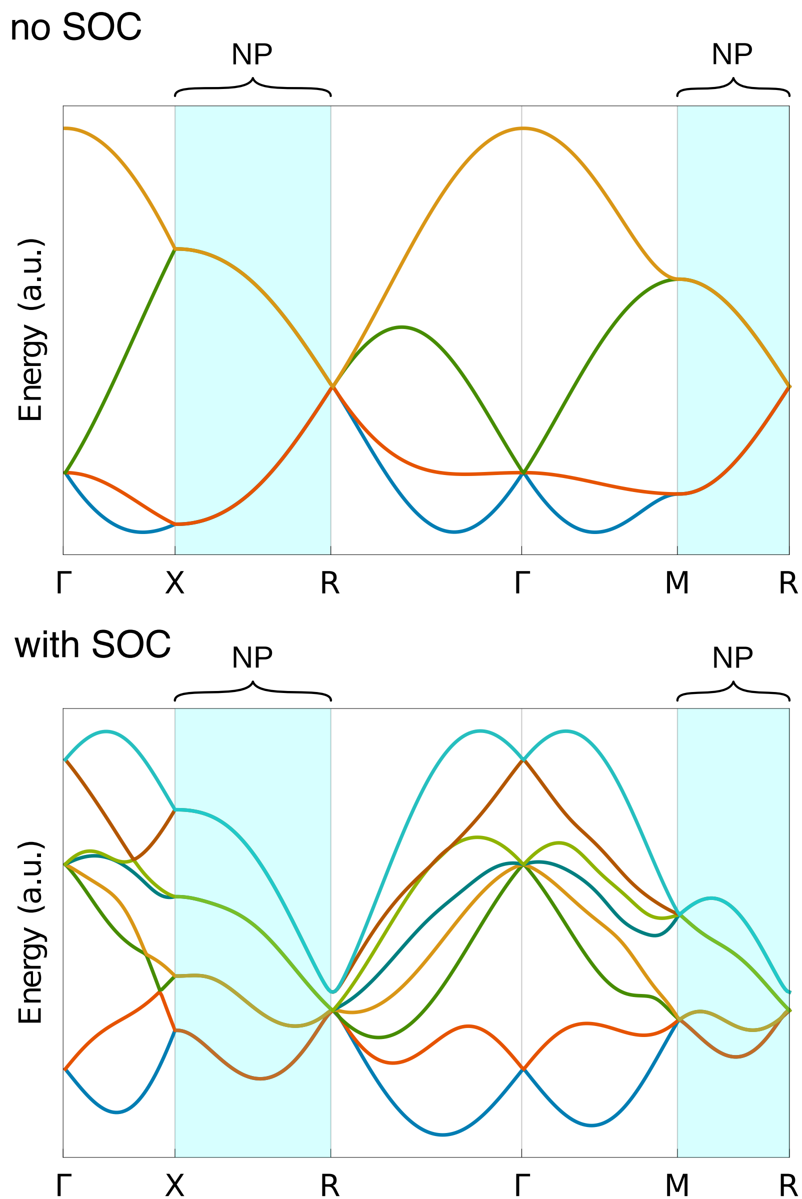

Electronic band structure & fermion-doubling theorem in CoSi

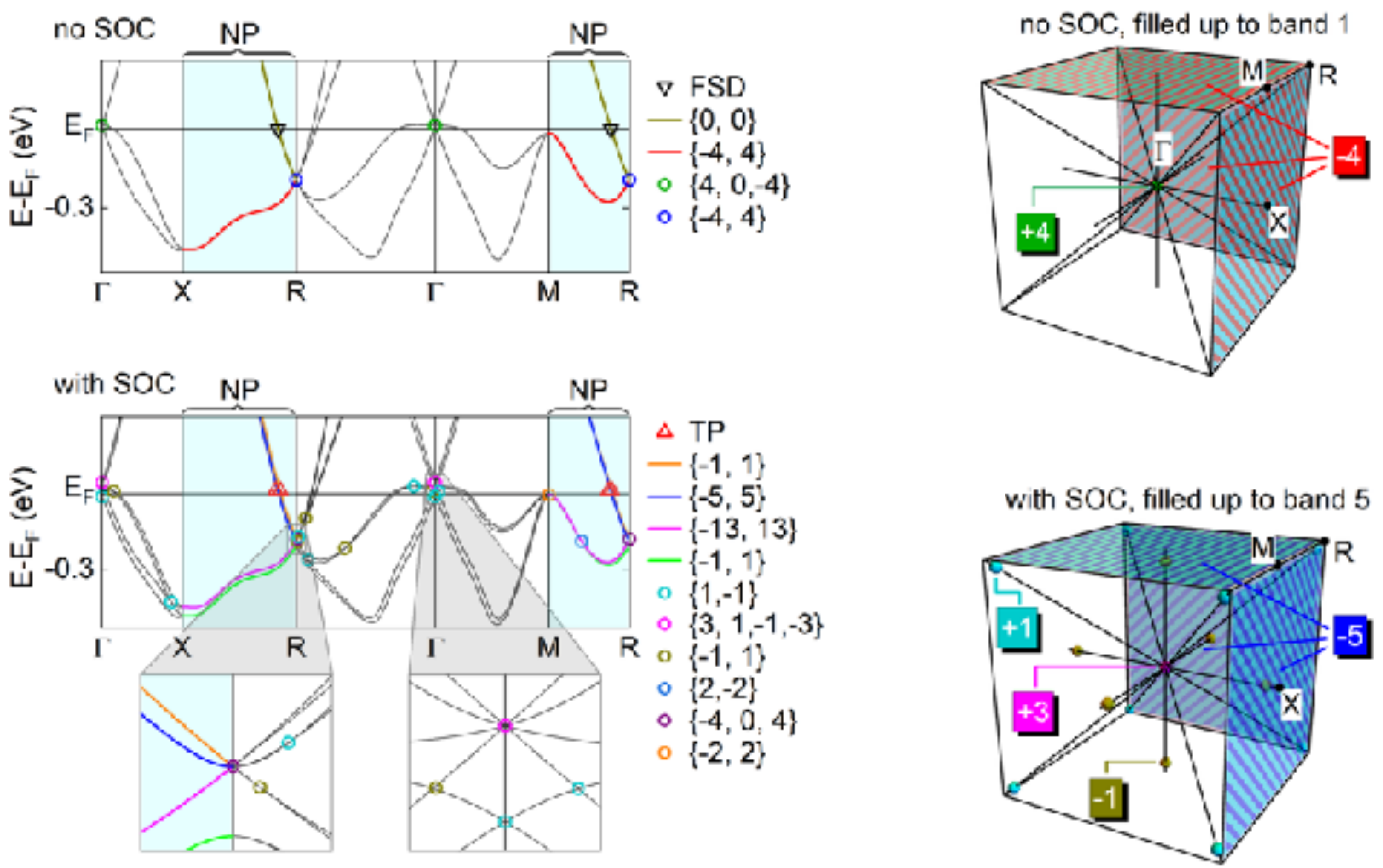

Shubnikov - de Haas Oscillations in CoSi

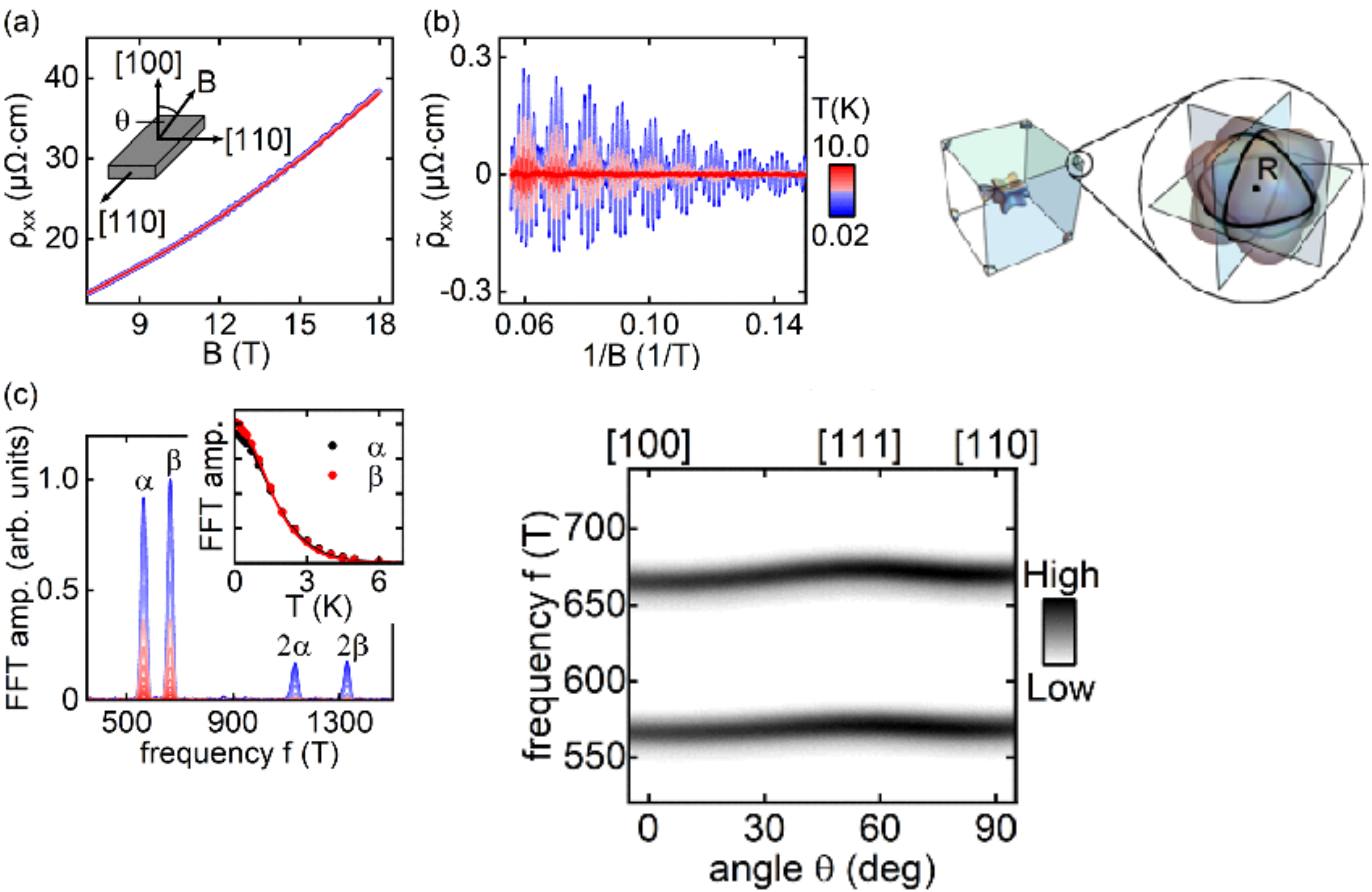

SdH Oscillations - Remarks on sample quality

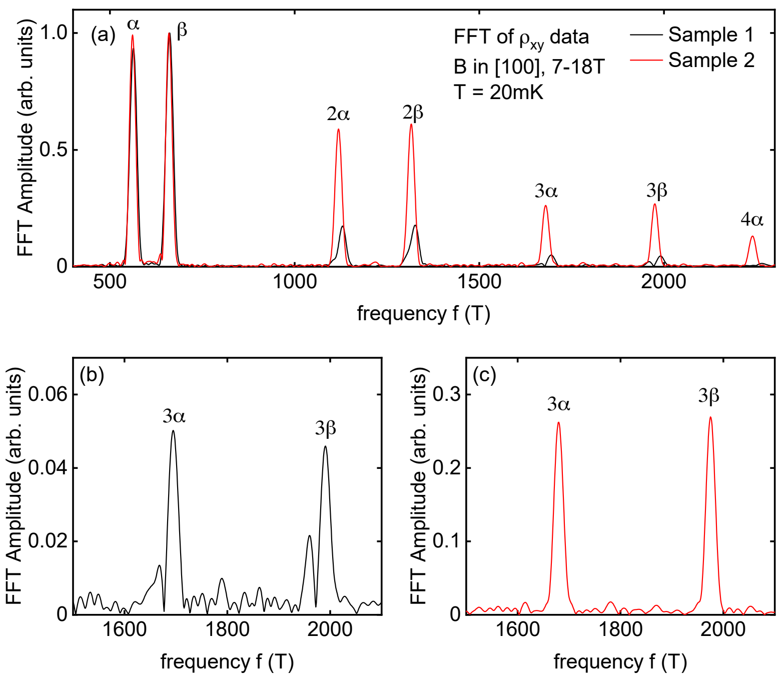

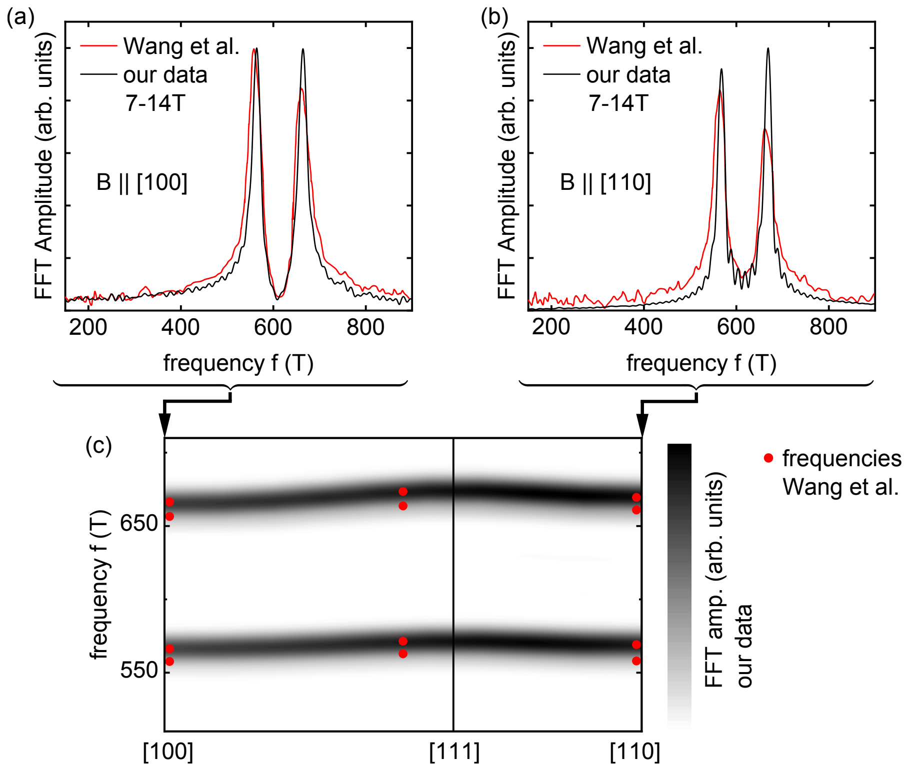

Effect of SOC and NPs on Shubnikov - de Haas branches

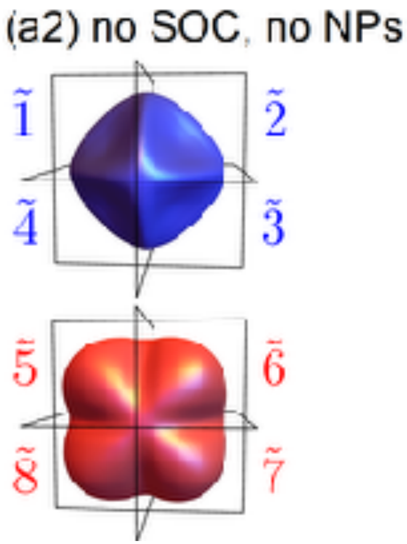

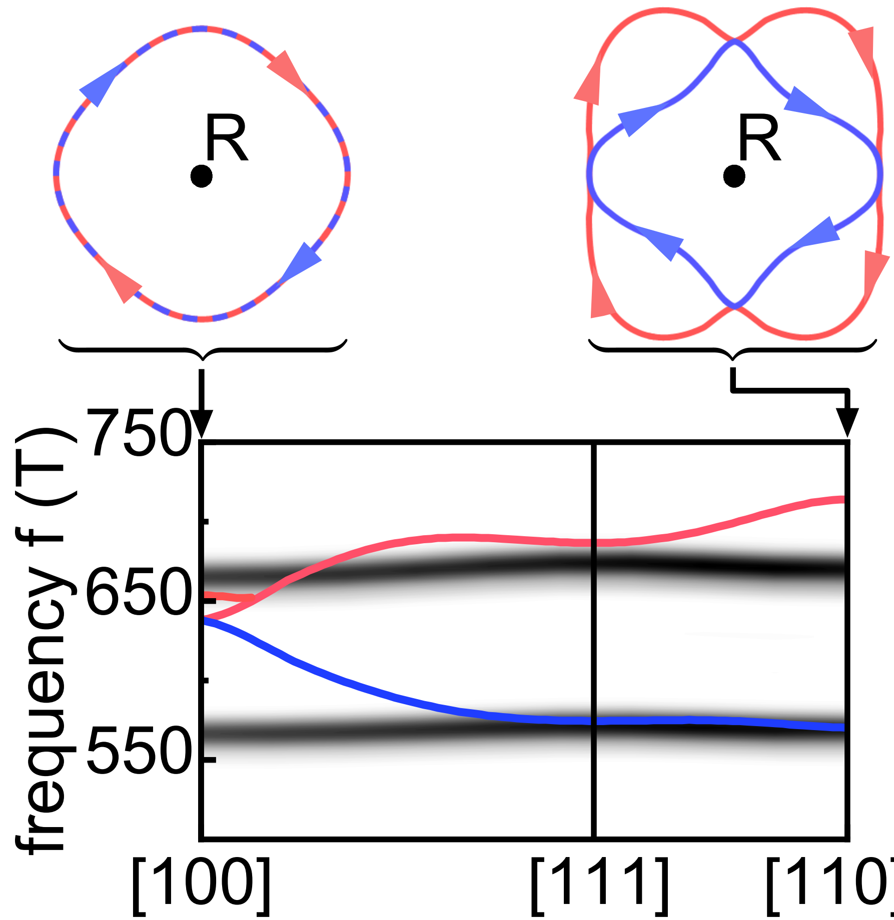

scenario proposed by
D.S. Wu et al., Chin. Phys. Lett. **36** 077102 (2019)
Xitong Xu et al., PRB **100** 045104 (2019)

Effect of SOC and NPs on Shubnikov - de Haas branches

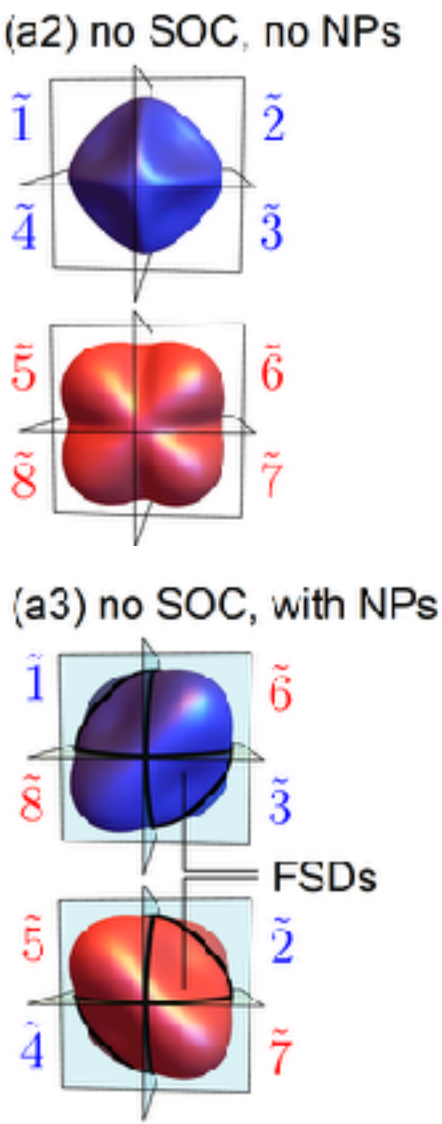

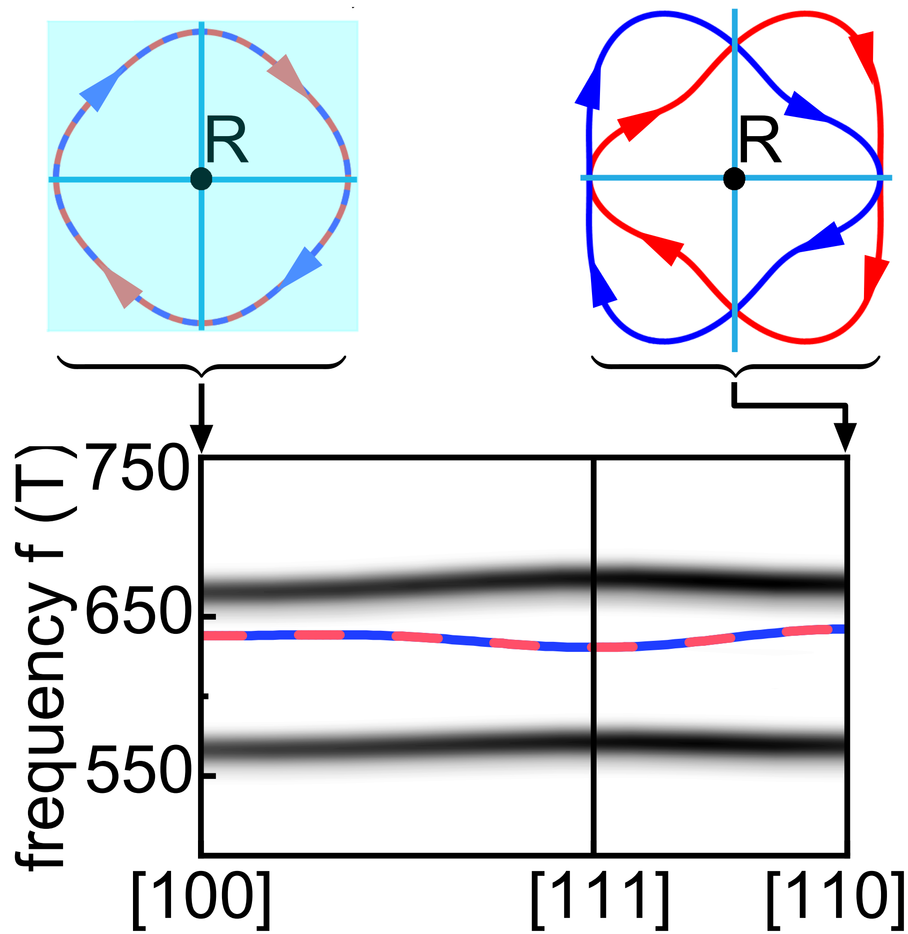

Effect of SOC and NPs on Shubnikov - de Haas branches

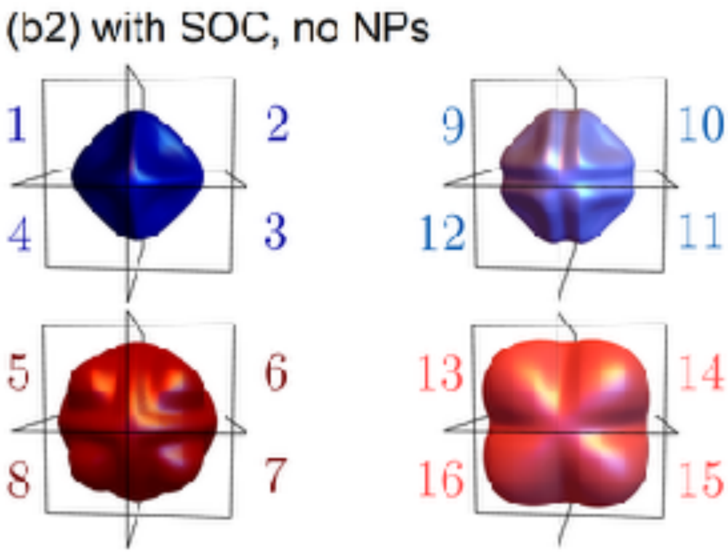

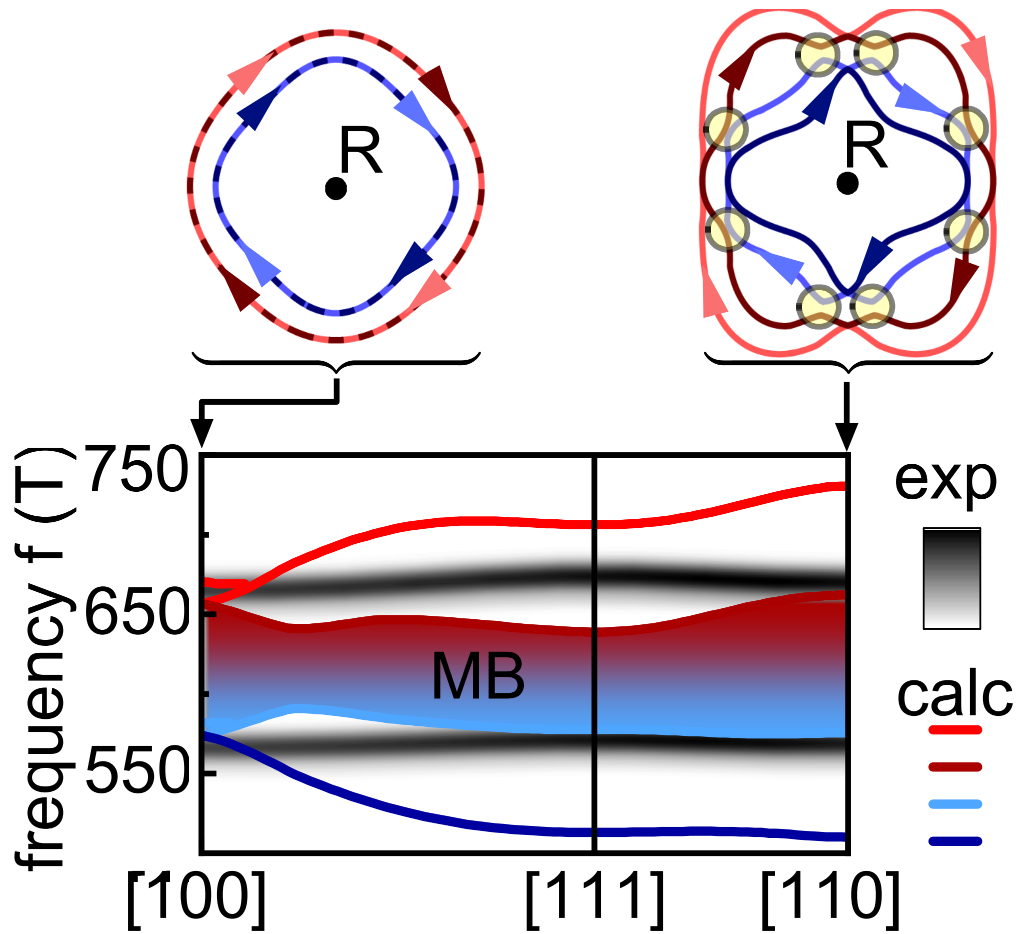

scenario proposed by

Huan Wang et al., PRB **102** 115129 (2020)

Effect of SOC and NPs on Shubnikov - de Haas branches

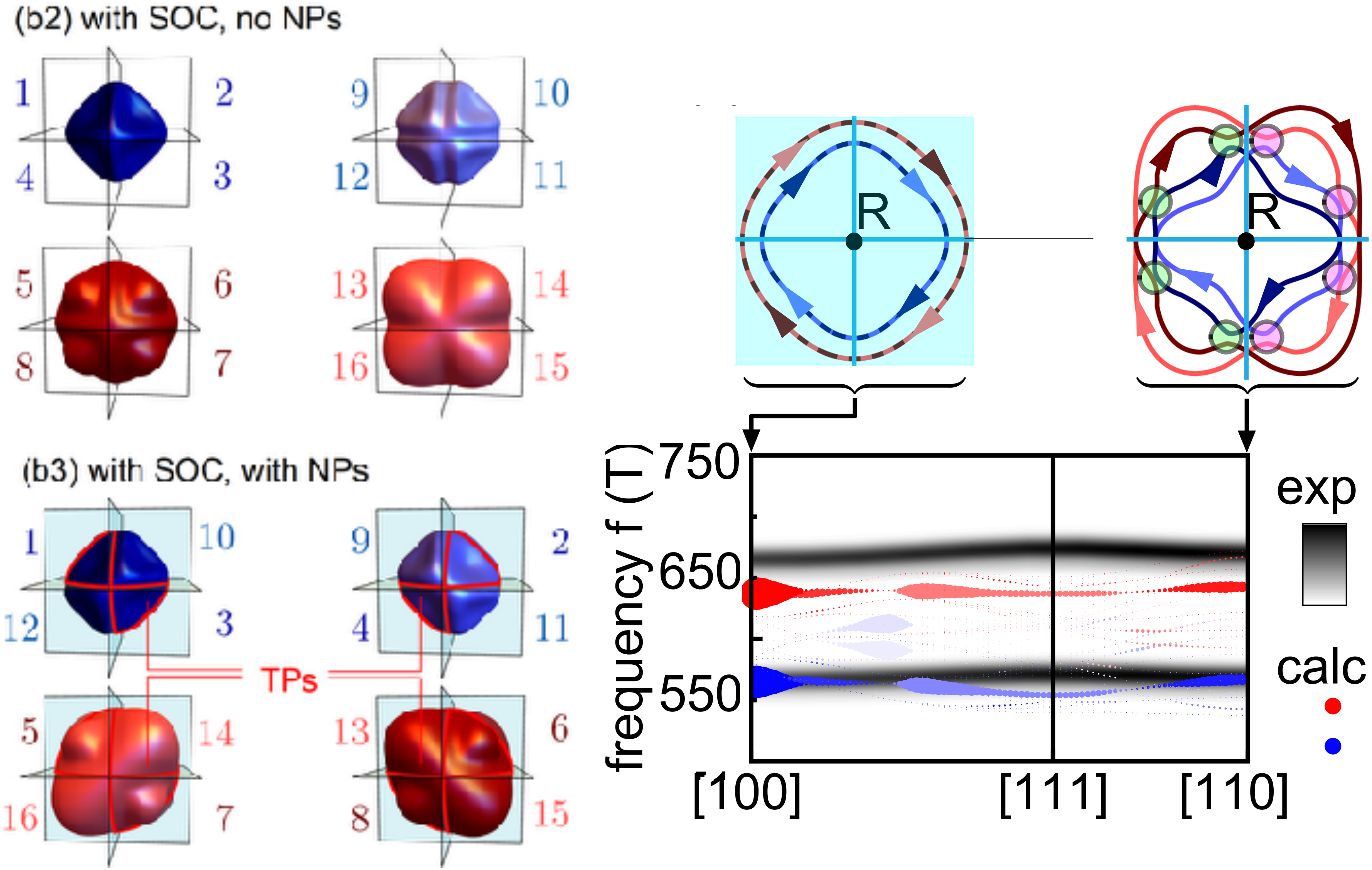

Topological Protectorates in MnSi

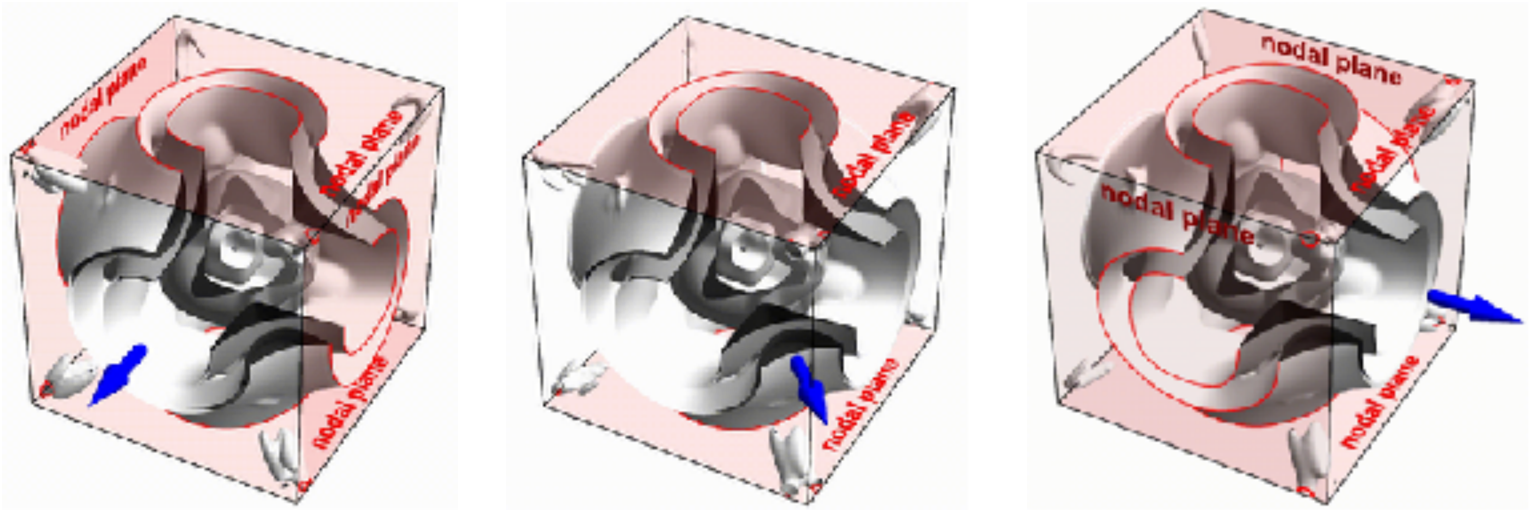

Weak Itinerant (Ferro)magnetism in MnSi

Dispersive Spin Fluctuations

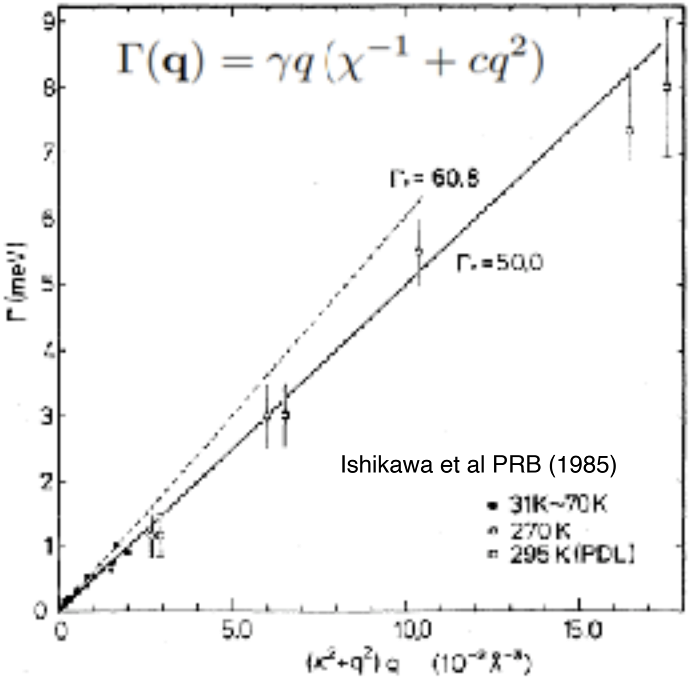

Spin Fluctuation Theory

$$T_c = 2.387cM_0^{3/2}\frac{(\hbar\gamma)^{1/4}}{k_B}$$

Property	Experiment	Present model
$\chi^{-1}(T)$ $2T_c \lesssim T \lesssim 10\,T_c$	Linear(c)	Linear(c,d)
T_c(K)	29.5(5)	31
p_{eff}/p_0(e)	5.5(4)	4.7

Lonzarich JMMM **45,** 43 (1984)
Lonzarich, Taileffer. J. Phys. Cond. Matter **18,** 4339 (1985)

Quantum Oscillations

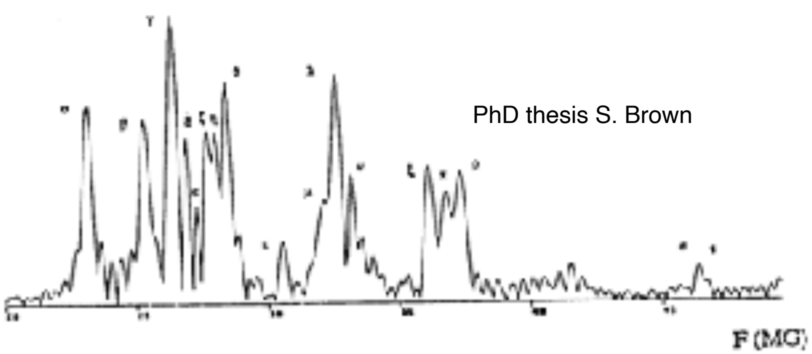

Landau Quasiparticles

We conclude that a reasonable case exists for describing the quasiparticles in MnSi as magnetic polarons with masses moderately enhanced by a factor of about five above the conventional band calculated masses. The polarisation cloud associated with these polarons is the spin density within the conduction electron sea itself.

Lonzarich JMMM **76,** 1 (1988)

Magnetic Phase Diagram of MnSi

field-polarized

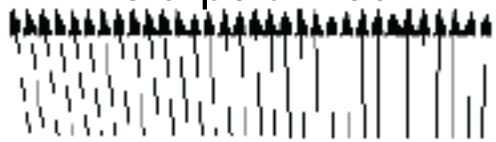

conical

skyrmion lattice

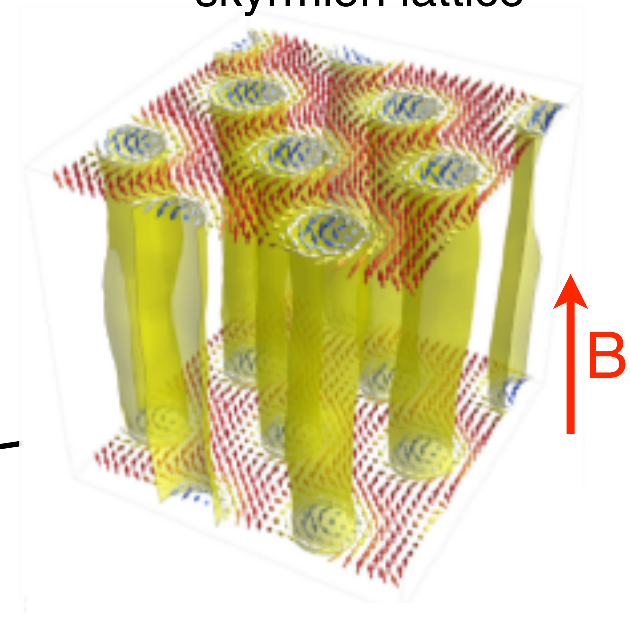

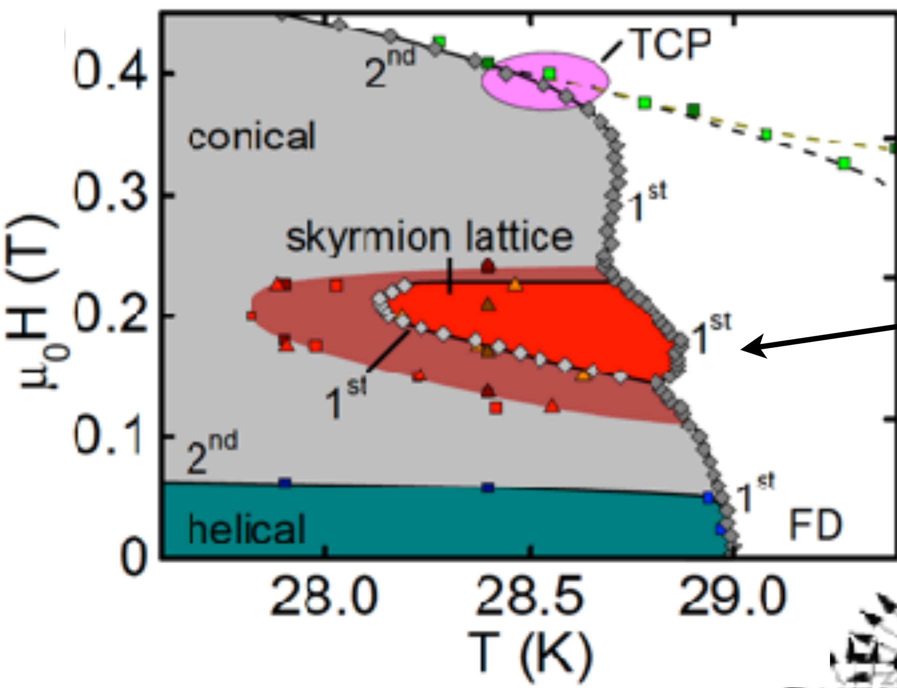

$$\phi = \frac{1}{4\pi}\vec{n}\cdot\frac{\partial\vec{n}}{\partial x}\times\frac{\partial\vec{n}}{\partial y}$$

winding number per unit cell:

$$\Phi = -1$$

skyrmions

helical

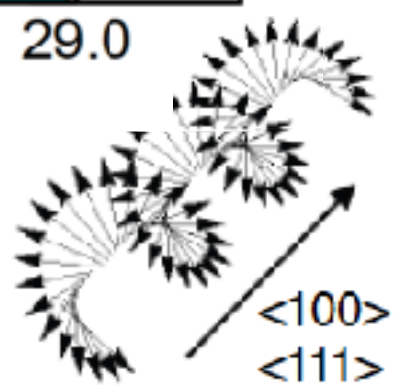

Mühlbauer et al, Science **323**, 915 (2009)
Jonietz, et al. Science (2010)
Bauer, Garst, CP, PRL **110**, 177207 (2013)

Calculated Hall-Effects in $Mn_{1-x}Fe_xSi$

Fermi surface of MnSi

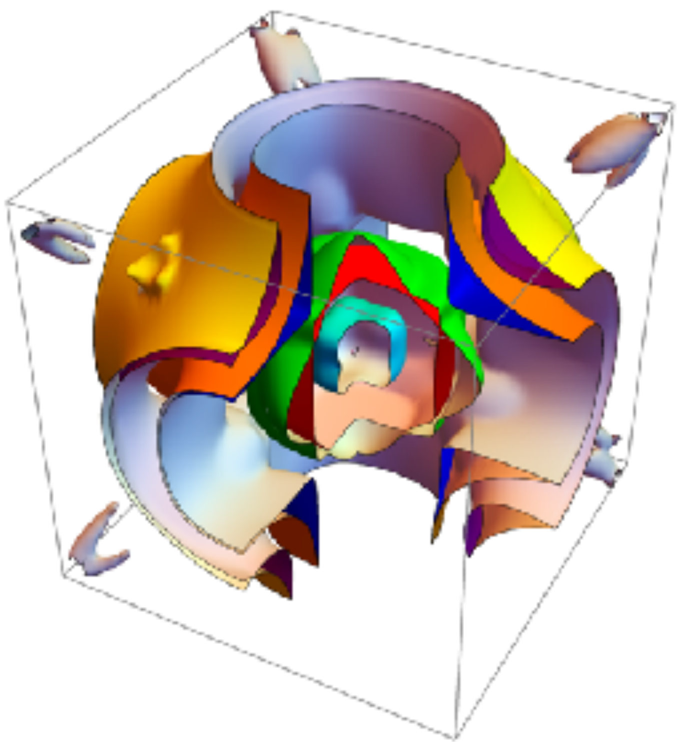

cf Jeong, Pickett, PRB **70**, 075114 (2004)
Wilde, et al., Nature **594**, 374 (2021)

DFT calculation (FLEUR, Jülich)

- virtual crystal approximation
- coherent potential approximation

intrinsic anomalous Hall conductivity
from Berry curvature

$$\sigma_z = \frac{e^2\hbar}{4\pi^3} \mathrm{Im} \int_{\mathrm{BZ}} d\mathbf{k} \sum_{n,m}^{o,e} \frac{\langle \psi_{n\mathbf{k}} | v_x | \psi_{m\mathbf{k}} \rangle \langle \psi_{m\mathbf{k}} | v_y | \psi_{n\mathbf{k}} \rangle}{(\varepsilon_{m\mathbf{k}} - \varepsilon_{n\mathbf{k}})^2}$$

cf Zhang et al. PRL **106** 117202 (2011)

topological Hall resistivity
from OHE in emergent magnetic field

$$\sigma_{\mathrm{xy}}^{\mathrm{OHE},s}(B^{\mathrm{z}}) = -\frac{e^3 B^{\mathrm{z}}}{VN} \sum_{\mathbf{k}n} \tau_s^2\, \delta(E_F - \varepsilon_{\mathbf{k}ns}) \times$$
$$\times \left[(v_{\mathbf{k}ns}^{\mathrm{x}})^2 m_{\mathbf{k}ns}^{\mathrm{yy}} - v_{\mathbf{k}ns}^{\mathrm{x}} v_{\mathbf{k}ns}^{\mathrm{y}} m_{\mathbf{k}ns}^{\mathrm{xy}} \right]$$

$$\rho_{yx}^{\mathrm{top}}(B^{\mathrm{eff}}) = \frac{\sigma_{\mathrm{xy}}^{\mathrm{OHE},\uparrow}(B^{\mathrm{eff}}) - \sigma_{\mathrm{xy}}^{\mathrm{OHE},\downarrow}(B^{\mathrm{eff}})}{(\sigma_{\mathrm{xx}}^{\uparrow} + \sigma_{\mathrm{xx}}^{\downarrow})^2}$$

cf Freimuth et al. PRB **88** 214409 (2013)

Phase Diagrams & Hall-Effect in $Mn_{1-x}Fe_xSi$

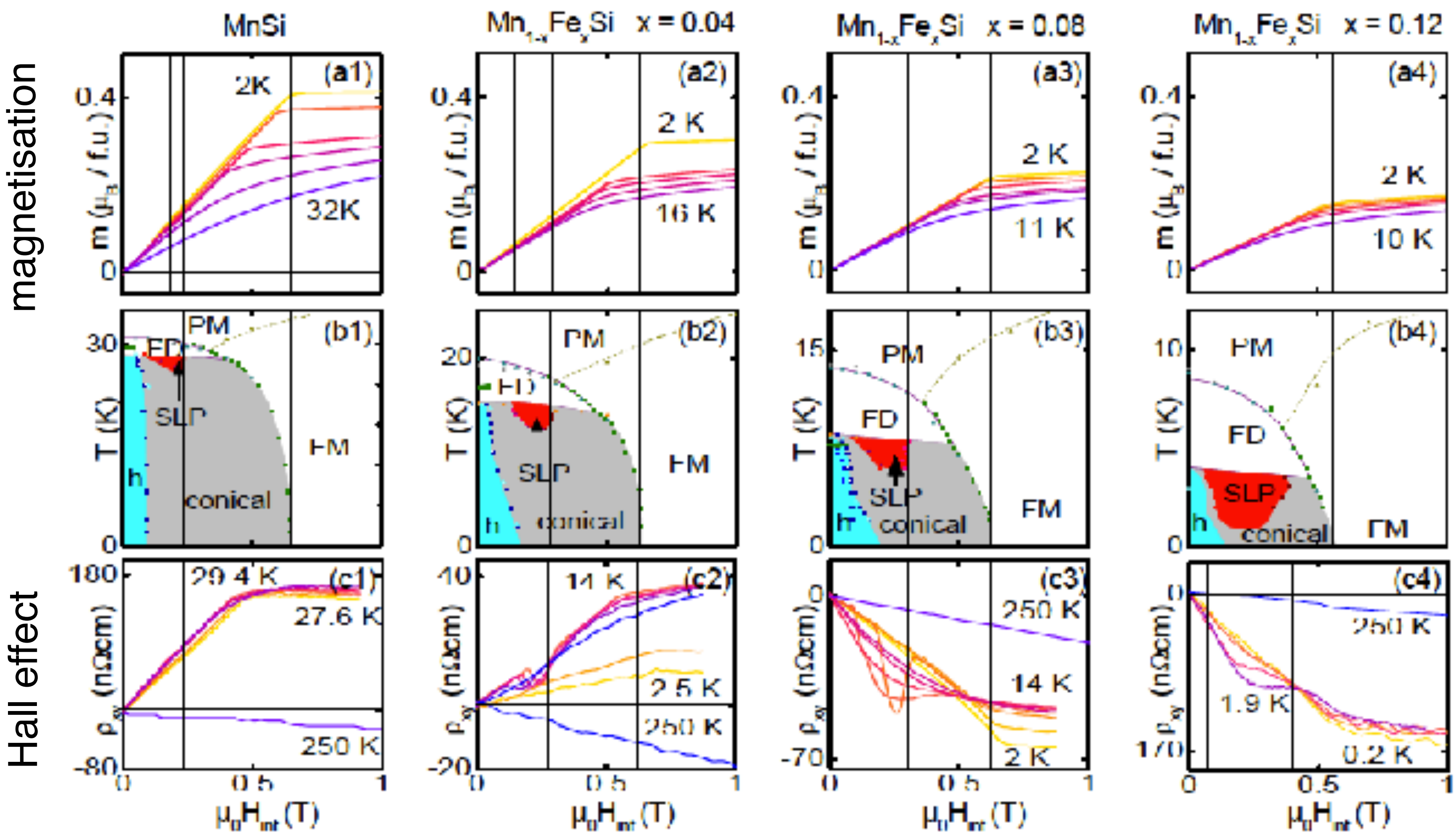

anomalous and topological Hall effect: large quantitative variation & change of sign

Franz, et al. PRL **112** 186601 (2014)
Bauer, et al. PRB **82** 064404 (2010)

see also Chapman et al. PRB **88** 214406 (2013)

Comparison of Experiment with Calculation in $Mn_{1-x}Fe_xSi$

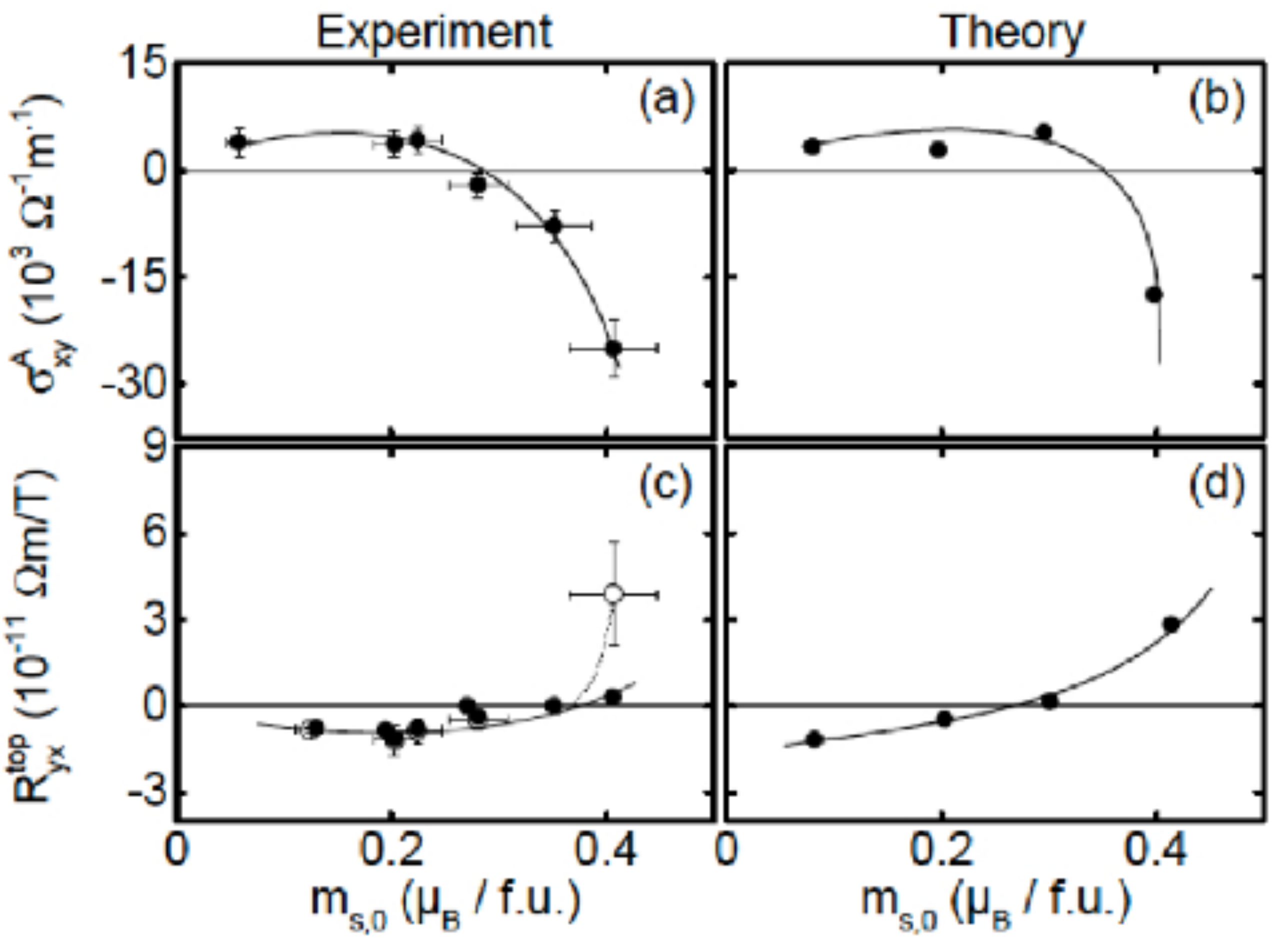

for T=0

origin of doping-dependence:
(1) consider paramagnetic MnSi
(2) doping induced reduction of DOS
(3) decrease and change of sign of OHE

Franz, et al. PRL **112** 186601 (2014)

Magnetic screw rotations, time-reversal symmetry & magnetic space groups

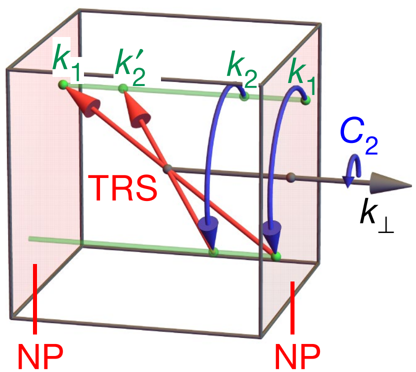

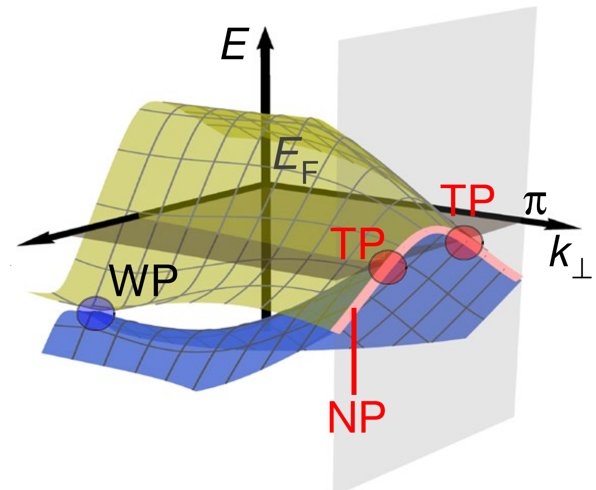

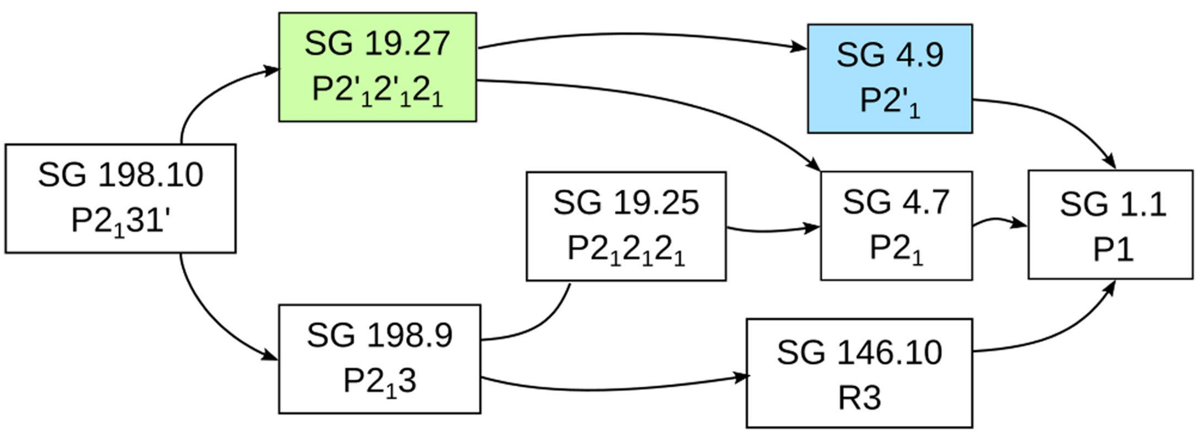

Band structure of ferromagnetic MnSi

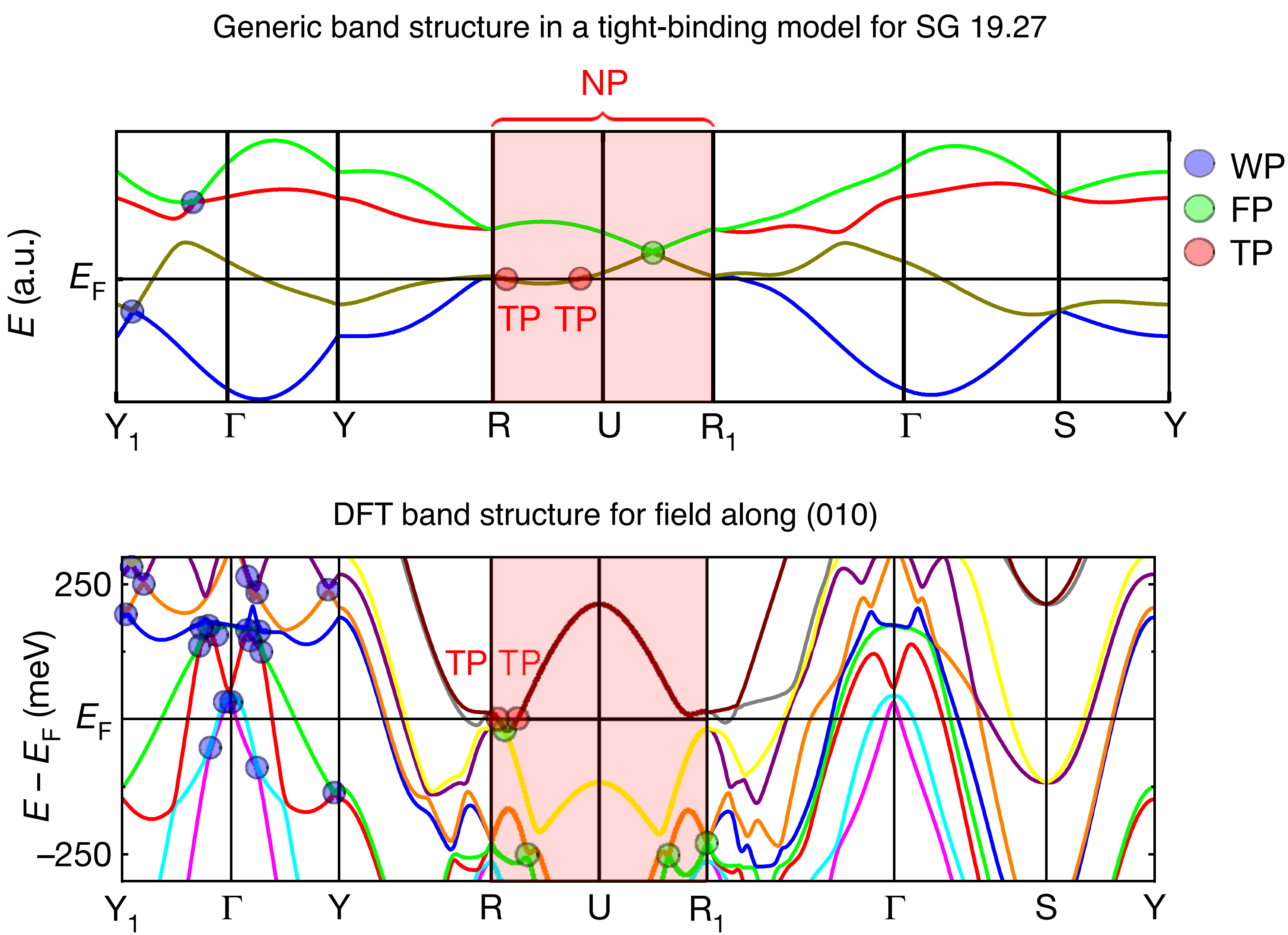

de Haas - van Alphen spectra in MnSi

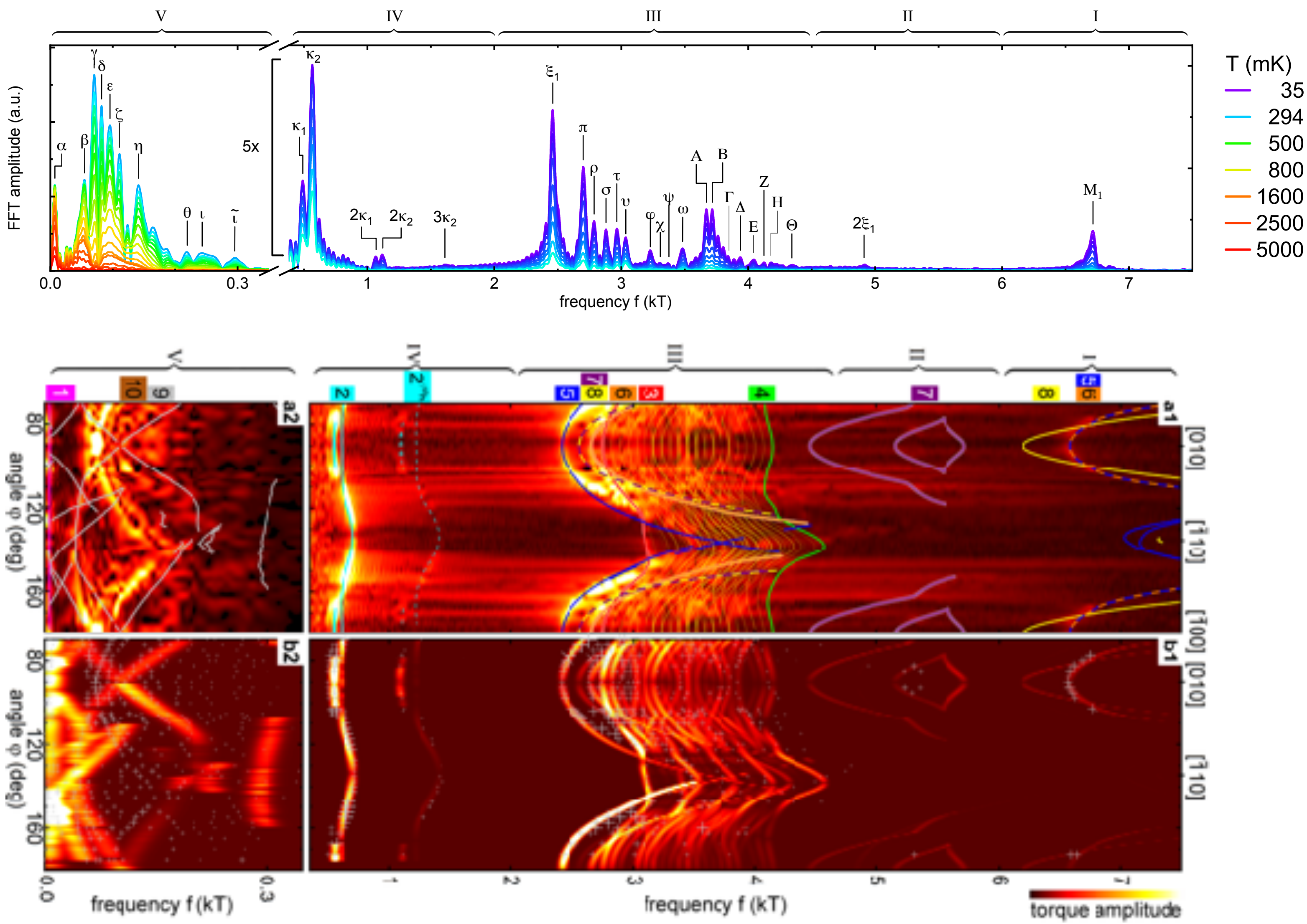

Assignment of dHvA branches & orbits to calculated Fermi surface

Branch	Orbit	$f_{exp.}$ [kT]	$f_{pred.}$ [kT]	m^* [m_e]	m_b [m_e]	$\frac{m^*}{m_b}$	φ [deg]
α	1Γ	0.007↘	0.068↘	0.4±0.1	0.1	4	82.5
β	9ΓR(1)	0.054	–↘	0.8±0.1	0.6	1.4	82.5
γ	9ΓR(2)	0.070	–↘	2.7±0.3	1.9	1.4	82.5
δ	9ΓR(3)	0.082	–↘	2.3±0.6	1.9	1.2	82.5
ϵ	9ΓR(4)	0.095	–↘	2.0±0.5	–	–	82.5
ζ	9ΓR(5)	0.110	–↘	2.4±0.4	–	–	82.5
η	9ΓR(6)	0.141	–↘	2.5±0.5	–	–	82.5
μ	9ΓR(7)	0.130	–↘	–	1.9	–	152.5
θ	9ΓR10R(1)	0.225	–↘	3.5±0.6	–	–	82.5
ι	9ΓR10R(2)	0.248	–↘	5.4±0.6	–	–	82.5
$\tilde{\iota}$	9ΓR10R(3))	0.290	–↘	5.4±0.6	~ 2.0	~ 2.7	82.5
κ_1	2Γ	0.488↘ (0.523)	0.369↘	6.3±0.6	1.1	6.0	82.5 (106)
κ_2	2ΓY(1)	0.566↘ (0.564)	0.371↘	6.2±0.1	1.1	5.9	82.5 (106)
κ_3	2ΓY(2)	0.641↘	0.411↘	6.5±0.5	1.2	5.6	106
$2\kappa_1$	$2\kappa_1$	1.065	$2f_{\kappa_1}$	14.2±0.8	$2m_{\kappa_1}$	–	82.5
$2\kappa_2$	$2\kappa_2$	1.120	$2f_{\kappa_2}$	14.0±0.6	$2m_{\kappa_2}$	–	82.5
$3\kappa_2$	$3\kappa_2$	1.610	$3f_{\kappa_2}$	16±6	$3m_{\kappa_2}$	–	82.5
ξ_1	5ΓY(1)	2.459↗ (2.576)	2.532↗	10.3±0.1	2.0	5.4	82.5 (165)
ξ_2	5ΓY(2)	2.653	–	–	–	–	165
$\o'$	7U8U	2.658	2.765↗	10.0±0.3	2.0	5.0	82.5
π	6ΓY	2.701↗	2.822↗	11.1±0.3	2.0	5.6	82.5
ρ	3Γ	2.786↘	2.891→	10.9±0.4	1.5	7.1	82.5
ρ'	3Γ4Γ(1)	2.833	2.934→	–	1.5	–	82.5
σ	3Γ4Γ(2)	2.879	2.976→	11.2±0.4	1.5	7.5	82.5
σ'	3Γ4Γ(3)	2.918	3.021→	–	–	–	82.5
τ	3Γ4Γ(4)	2.966	3.019→	10.2±0.4	1.5	6.8	82.5
υ	3Γ4Γ(5)	3.034↘	3.061↘	8.7±0.3	1.5	5.9	82.5
υ'	3Γ4Γ(6)	3.105	3.231→	–	–	–	82.5
φ	3Γ4Γ(7)	3.229	3.453→	13.2±0.4	–	–	82.5
χ'	3Γ4Γ(8)	3.350	3.583→	–	–	–	82.5
ψ	3Γ4Γ(9)	3.450	3.715→	11.6±0.6	–	–	82.5
ω	3Γ4Γ(10)	3.485↗	3.626→	11.6±0.6	–	–	82.5
A	3Γ4Γ(11)	3.671	3.931→	13.6±0.1	–	–	82.5
B	3Γ4Γ(12)	3.717↘	4.017→	13.7±0.3	–	–	82.5
Γ'	3Γ4Γ(13)	3.840	4.323↗	–	3.2	–	82.5
Δ	3Γ4Γ(14)	3.940	4.366→	14±1	3.2	4.4	82.5
E	3Γ4Γ(15)	4.040	4.409→	17±4	3.2	5.5	82.5
Z	3Γ4Γ(16)	4.120	4.451→	15±3	3.2	4.7	82.5
H	4Γ	4.180	4.493→	16±5	3.1	5.1	82.5
Θ	7ΓY(1)	4.350	4.569	15±5	4.0	3.8	82.5
$2\xi_1$	$2\xi_1$	4.920	$2f_{\xi_1}$↘	24±5	$2m_{\xi_1}$	–	82.5
K	7ΓY(2)	5.304	5.179↘	–	4.2	–	85
Λ	7Y	5.304	5.481↘	–	3.4	–	85
M_1	5U6U	6.715↘ (6.634)	6.627↘	15.1±0.2	~2.8	5.4	82.5 (175)
M_2	5U6U	6.587	–	–	–	–	175
–	8ΓY	–	6.610↘	–	4.0	–	–

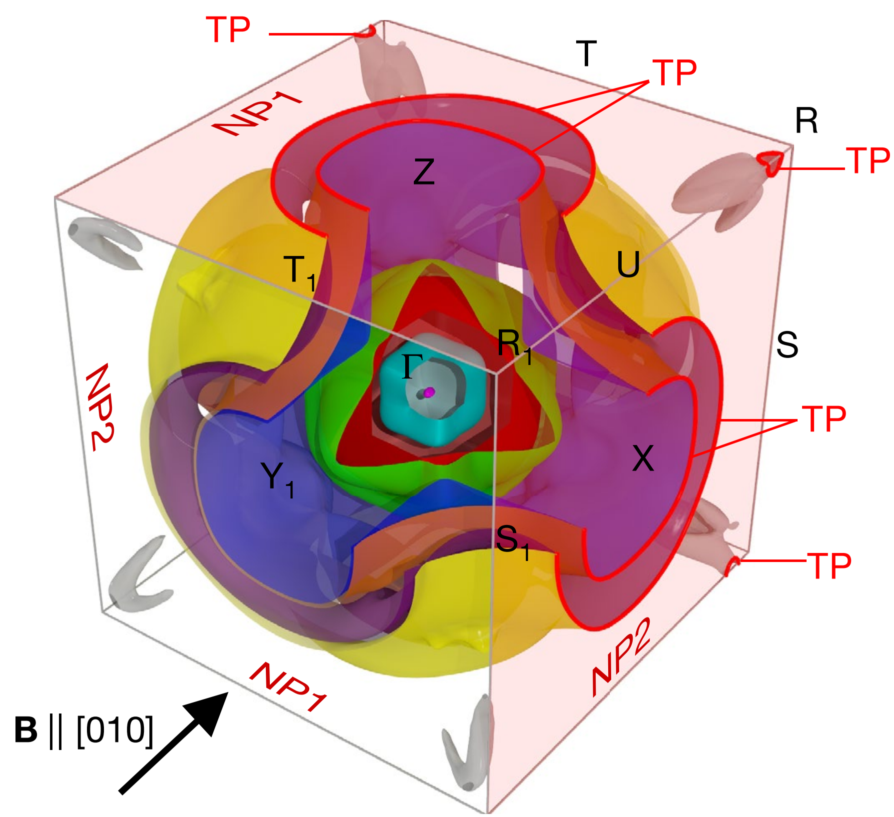

Key properties of Fermi surface sheets

sheet no.	topology	location	carrier type	spin character	$f(B)$-shift
			e/h		
1	pocket	Γ-centered	h	majority	↘
2	pocket	Γ-centered	h	majority	↘
3	pocket	Γ-centered	h	mixed	-
4	pocket	Γ-centered	h	mixed	-
5	jungle-gym	-	necks: h	minority	necks: ↗
			loops: e	minority	loops: ↘
6	jungle-gym	-	necks: h	minority	necks: ↗
			loops: e	minority	loops: ↘
7	jungle-gym	-	necks: h	majority	necks: ↘
			loops: e	majority	loops: ↗
8	jungle-gym	-	necks: h	majority	necks: ↘
			loops: e	majority	loops: ↗
9	pockets	Γ-*R*	e	minority	↗
10	pocket/none	*R*	h	minority	↘

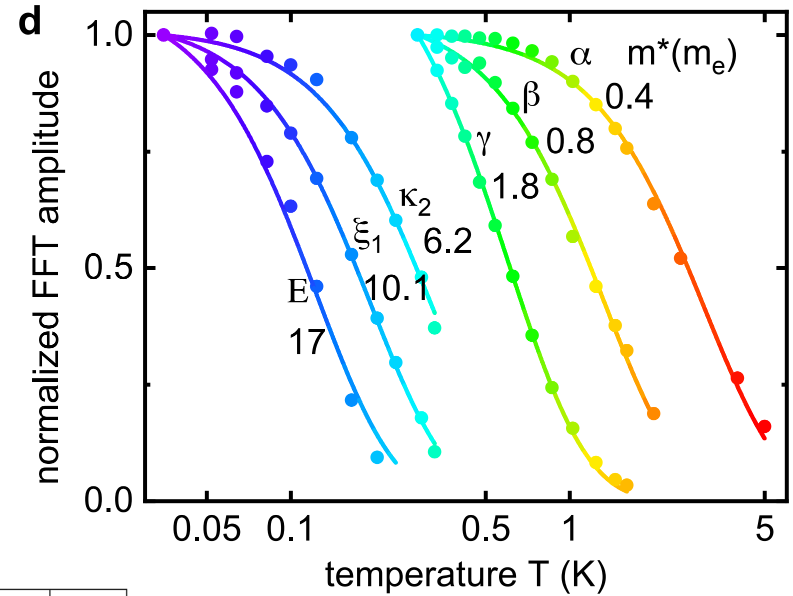

sheet no.	$D(E_F)$	E_F-shift	$D(E_F + E_F\text{-shift})$	γ	m^*/m_b	γ^*
	(states/(eV u.c.))	(mJ/(mol K^2))		(mJ/(mol K^2))		
1	0.011	27	0.001	10^{-4}	~ 5	0.004
2	0.084	–20	0.11	0.07	5.9	0.41
3	0.36	8.5	0.36	0.21	7.3	1.53
4	0.62	9.5	0.62	0.36	5.0	1.80
5	1.66	4	1.66	0.98	5.5	5.39
6	1.74	4	1.74	1.03	5.6	5.77
7	2.44	–4	2.47	1.46	5	7.3
8	1.74	–4	1.77	1.04	~ 5	5.2
9	1.09	–11	0.84	0.5	~ 1.5	0.75
10	0.36	–11	0 – 0.08	0 – 0.05	-	-
sum	**10.1**		**9.65**	**5.65**	**5.1**	**28.15**
					specific heat experiment[32]:	**28**

Extremal orbits and spectroscopic signatures of NPs and TPs

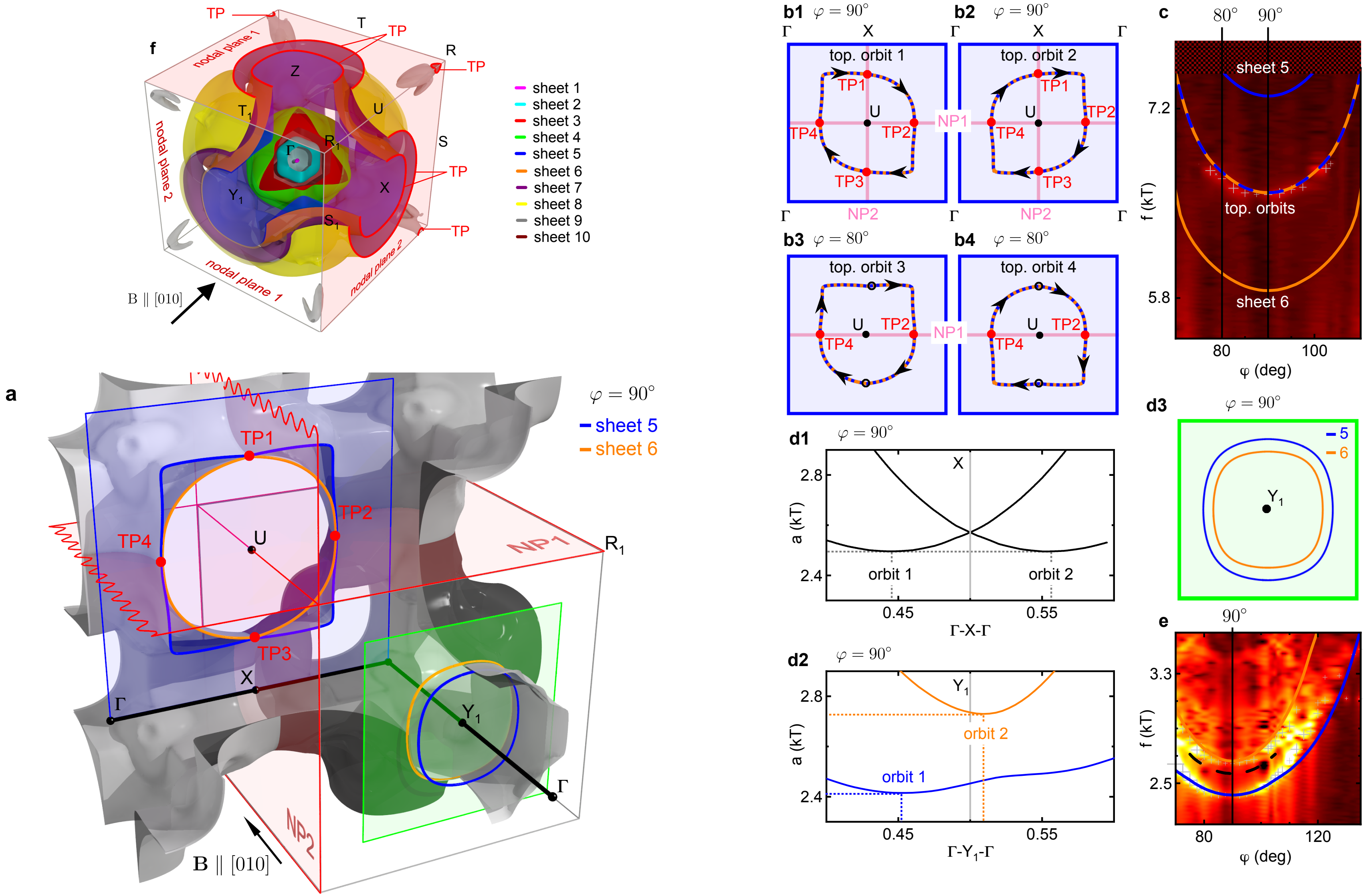

Momentum dependence of screw-rotation eigenvalues

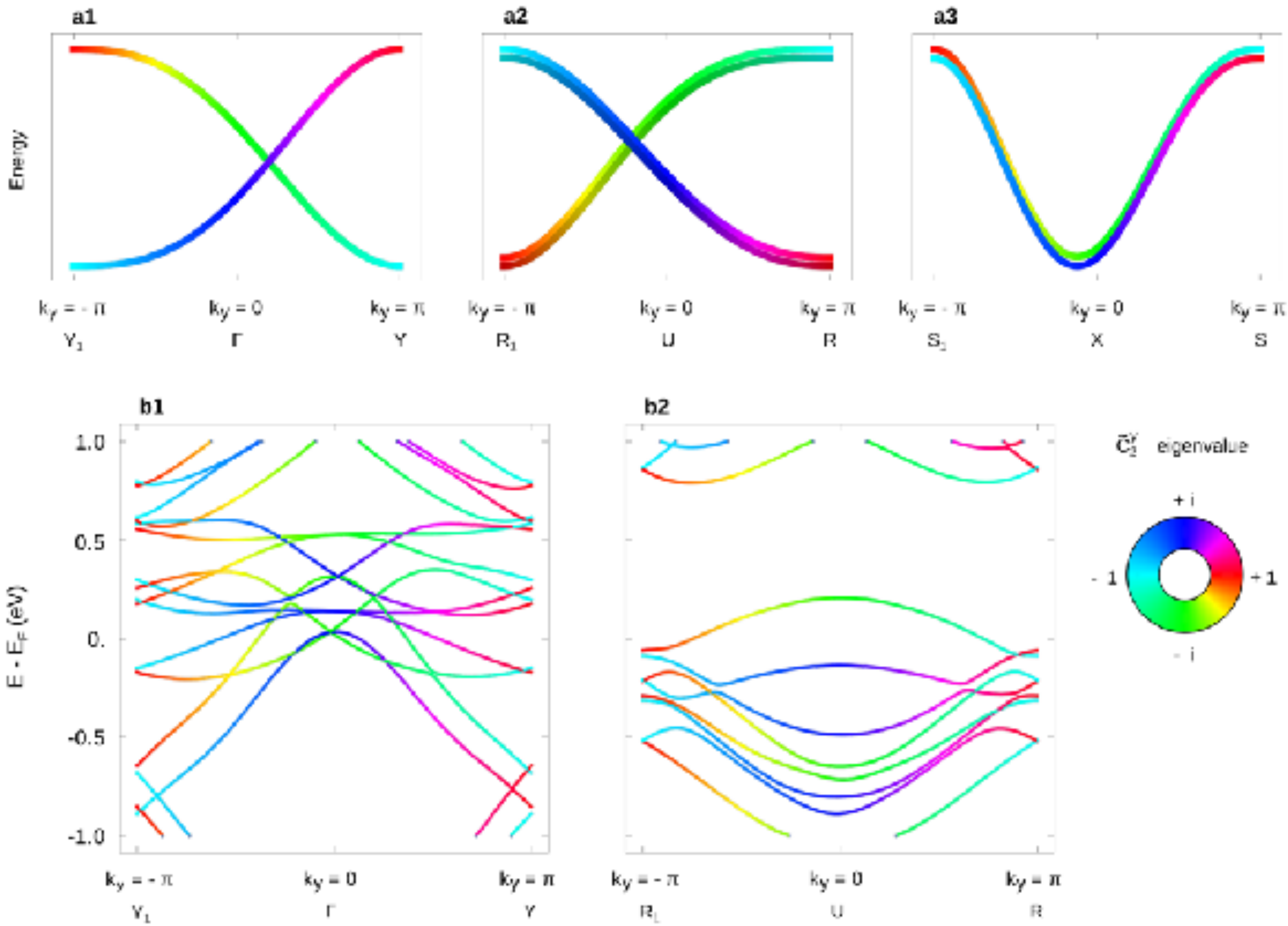

Berry curvature on a FS in a tight-binding model

SG 19.27

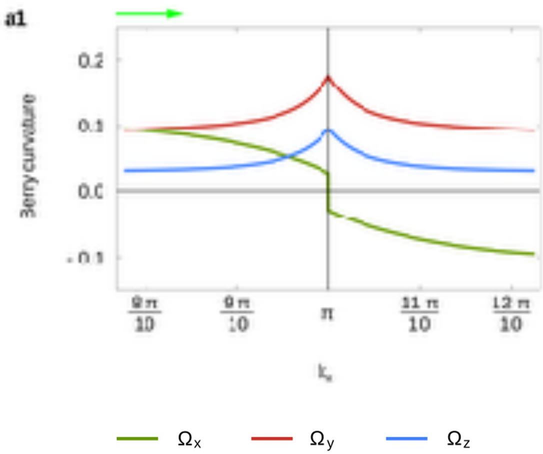

SG 4.9

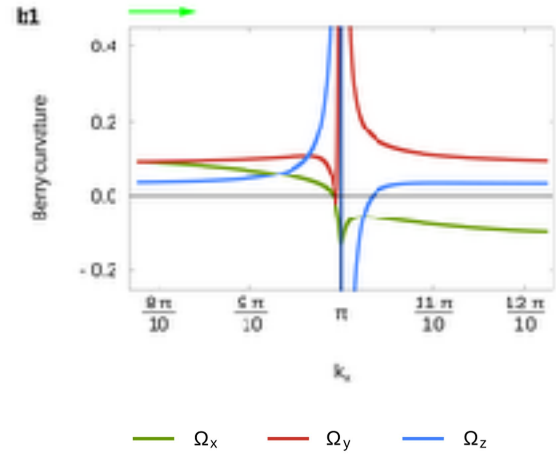

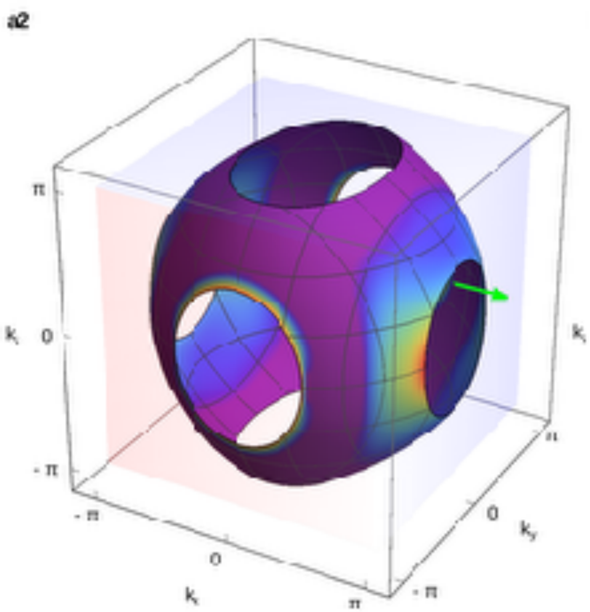

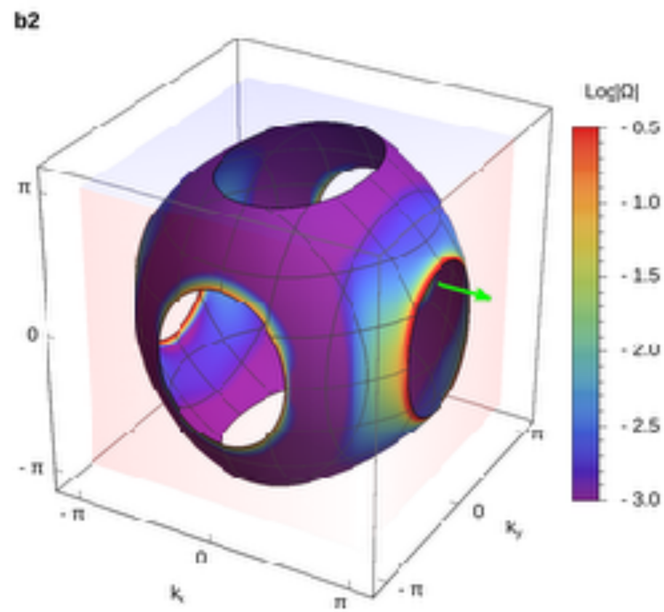

Topological surface states on a (010) surface in SG 19.27

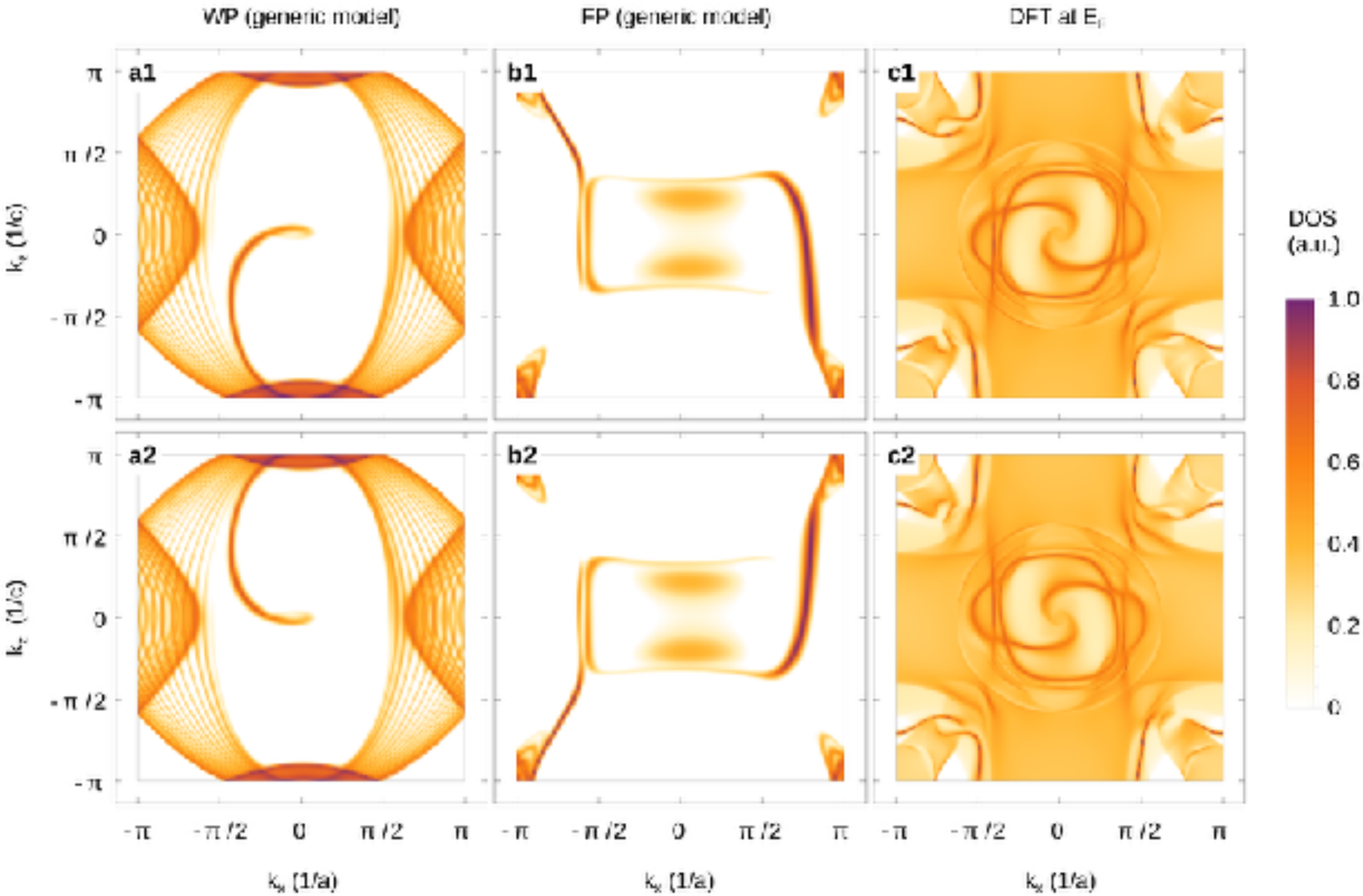

Magnetic space groups with symmetry enforced nodal planes

4.8 [t]	17.8 [t]	18.17 [t]	19.26 [**T**]	20.32 [t]	26.67	29.100	31.124	33.145
36.173	76.8 [t]	78.20 [t]	90.96 [t]	91.104 [t]	92.112 [**T**]	94.128 [**T**]	95.136 [t]	96.144 [**T**]
113.268	114.276	169.114 [t]	170.118 [t]	173.130 [t]	178.156 [t]	179.162 [t]	182.180 [t]	185.198
186.204	198.10 [**T**]	212.60 [**T**]	213.64 [**T**]					

4.9 [t]	11.54	14.79	17.10 [t]	18.18 [t]	18.19 [t]	19.27 [**T**]	20.34 [t]	26.68
26.69	29.101	29.102	31.125	31.126	33.146	33.147	36.174	36.175
51.294	51.296	52.310	52.311	53.327	53.328	54.342	54.344	55.357
55.358	56.369	56.370	57.382	57.383	57.384	58.397	58.398	59.409
59.410	60.422	60.423	60.424	61.436	62.446	62.447	62.448	63.463
63.464	64.475	64.476	90.98 [t]	90.99 [t]	92.114 [**T**]	92.115 [**T**]	94.130 [**T**]	94.131 [t]
96.146 [**T**]	96.147 [**T**]	113.269	113.271 [t]	114.277	114.279 [t]	127.390	127.393	128.402
128.405	129.414	129.417	130.426	130.429	135.486	135.489	136.498	136.501
137.510	137.513	138.522	138.525	169.115 [t]	170.119 [t]	173.131 [t]	176.147	178.157 [t]
178.158 [t]	179.163 [t]	179.164 [t]	182.181 [t]	182.182 [t]	185.199	185.200	186.205	186.206
193.258	193.259	194.268	194.269					

3.5 [t]	3.6 [t]	4.10 [t]	16.4 [t]	16.5 [t]	16.6 [**T**]	17.11 [t]	17.13 [t]	17.14 [**T**]
17.15 [**T**]	18.20 [t]	18.21 [**T**]	18.22 [**T**]	18.24 [t]	19.28 [**T**]	19.29 [t]	20.36 [t]	21.42 [t]
21.44 [t]	25.61	25.64	25.65	26.71	26.72	26.76	27.82	27.85
27.86	28.94	28.95	28.96	28.98	29.104	29.105	29.109	30.118
30.119	30.120	30.122	31.128	31.129	31.133	32.139	32.142	32.143
33.149	33.150	33.154	34.161	34.162	34.164	35.169	35.171	36.178
37.184	37.186	75.4 [t]	75.6 [t]	76.11 [t]	77.16 [t]	77.18 [t]	78.23 [t]	81.36 [t]
81.38 [t]	89.92 [t]	89.93 [t]	89.94 [**T**]	90.100 [**T**]	90.102 [t]	91.109 [**T**]	91.110 [**T**]	92.116 [**T**]
92.117 [t]	93.124 [t]	93.125 [**T**]	93.126 [**T**]	94.132 [**T**]	94.134 [t]	95.141 [**T**]	95.142 [**T**]	96.148 [**T**]
96.149 [t]	99.168	99.170	100.176	100.178	101.184	101.186	102.192	102.194
103.200	103.202	104.208	104.210	105.216	105.218	106.224	106.226	111.256
111.257	111.258	112.264	112.265	112.266	113.272	113.274	114.280	114.282
115.288	115.290	116.296	116.298	117.304	117.306	118.312	118.314	168.112 [t]
171.124 [t]	172.128 [t]	177.154 [t]	180.172 [t]	181.178 [t]	183.190	184.196	195.3 [**T**]	207.43 [**T**]
208.47 [**T**]	215.73	218.84						

Table listing all magnetic SGs with symmetry-enforced NPs. The list is grouped into three blocks: 32 SGs with time-reversal symmetry (describing non-magnetic materials), 94 SGs without time-reversal symmetry (describing ferro- or ferrimagnets), and 129 SGs with a symmetry that combines time-reversal symmetry with a translation (describing antiferromagnets). For the NPs to have non-zero topological charge, the SG must be chiral (labelled by '[t]' or '[**T**]'). The 33 SGs labelled by '[**T**]' have NPs whose topological charge is enforced to be non-zero by symmetry, as discussed in Supplementary Note 3.

Summary

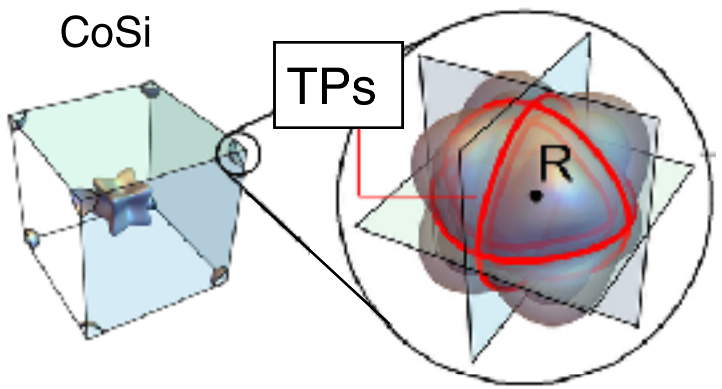

CoSi
TPs
R

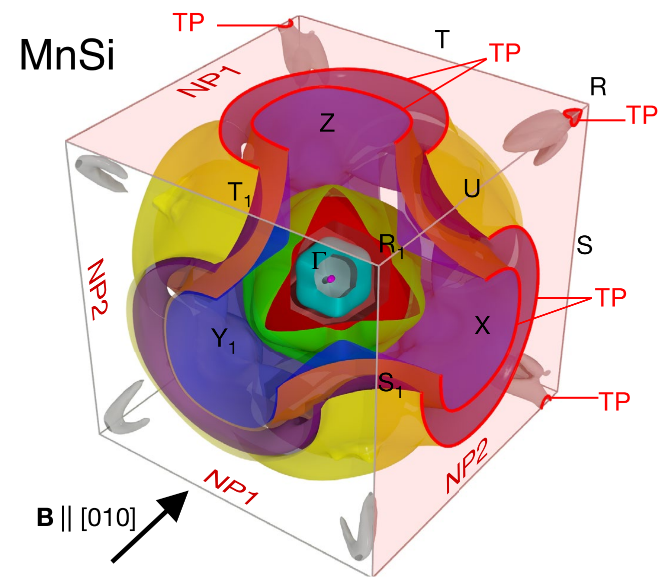

MnSi
TP
T
TP
R
TP
NP1
Z
T1
U
R1
S
Γ
NP2
TP
Y1
X
S1
TP
NP2
NP1
B || [010]